

# Xijiao Dihuang Decoction for Sepsis-Induced Acute Lung Injury: Network Pharmacology and Molecular Dynamics Insights

Jiaqi Xu <sup>1-3,\*</sup>, Conghan Jiao <sup>2-4,\*</sup>, Haiwei Du <sup>2,5</sup>, Xiaojing Guo <sup>1-3</sup>, Mutian Wang <sup>1-3</sup>, Yuening Ma <sup>1,2</sup>, Yanzhong Yin <sup>1,2</sup>, Min Liu <sup>1,2</sup>, Rongjiang Shao <sup>2,5</sup>

<sup>1</sup>Department of Infectious Diseases, the First Teaching Hospital of Tianjin University of TCM, Tianjin, People's Republic of China; <sup>2</sup>National Clinical Research Center for Chinese Medicine Acupuncture and Moxibustion, Tianjin, People's Republic of China; <sup>3</sup>Graduate School, Tianjin University of Traditional Chinese Medicine, Tianjin, People's Republic of China; <sup>4</sup>Department of Hematology, the First Teaching Hospital of Tianjin University of TCM, Tianjin, People's Republic of China; <sup>5</sup>Department of General Surgery, the First Teaching Hospital of Tianjin University of TCM, Tianjin, People's Republic of China

\*These authors contributed equally to this work

Correspondence: Rongjiang Shao, Department of General surgery, The First Teaching Hospital of Tianjin University of TCM, No. 88, Changling Road, Xiqing District, Tianjin, 300381, People's Republic of China, Tel +86 13920987128, Email 13920987128@163.com; Min Liu, Department of Infectious Diseases, The First Teaching Hospital of Tianjin University of TCM, No. 88, Changling Road, Xiqing District, Tianjin, 300381, People's Republic of China, Tel +86 13132296378, Email liumintcm@163.com

**Objective:** This study investigates the therapeutic mechanisms of Xijiao Dihuang Decoction (XJDHD) in sepsis-induced acute lung injury (SALI) through an integrated approach, including network pharmacology, molecular docking, molecular dynamics simulations, and in vitro experiments.

**Methods:** Network pharmacology identified active ingredients and targets in Xijiao Dihuang Decoction. Molecular docking and dynamics simulations evaluated binding affinity and stability with key targets. In vitro experiments on LPS-stimulated A549 cells substantiated Xijiao Dihuang Decoction's anti-inflammatory, antioxidant, and anti-apoptotic effects.

**Results:** Network pharmacology identified 20 active components among 182 Sepsis-Induced Acute Lung Injury targets. Molecular docking revealed strong binding affinity (binding energies  $\leq -5.0$  kcal/mol) for  $\beta$ -sitosterol with AKT1 and TNF. Molecular dynamics confirmed the complex stability. In vitro experiments demonstrated that Xijiao Dihuang Decoction significantly reduced inflammatory cytokines IL-6, TNF- $\alpha$ , and IL-1 $\beta$  ( $p < 0.001$ ), increased SOD and CAT mRNA ( $p < 0.05$ ), downregulated MyD88 mRNA ( $p < 0.05$ ), and modulated apoptosis-related proteins (Bax, Bcl-2, Cleaved-Caspase-3;  $p < 0.05$ ). The modulation of the PI3K/Akt pathway was confirmed by p-PI3K and p-Akt expression ( $p < 0.05$ ).

**Conclusion:** Xijiao Dihuang Decoction exhibits therapeutic efficacy in treating Sepsis-Induced Acute Lung Injury through its anti-inflammatory, antioxidant, and anti-apoptotic effects, and by modulating the PI3K/Akt pathway. This study provides experimental evidence for Xijiao Dihuang Decoction's mechanisms, highlighting its potential. However, additional in vivo and clinical investigations are required to validate its efficacy.

**Keywords:** Xijiao Dihuang Decoction, sepsis-induced acute lung injury, network pharmacology, mechanism of action, PI3K/Akt signaling pathway, anti-inflammatory, antioxidant, anti-apoptotic

## Introduction

Sepsis, a multiple-organ-dysfunction syndrome resulting from dysregulated systemic immune responses to infection, is a primary cause of mortality among ICU patients. Studies suggest that sepsis exhibits high incidence and mortality rates in ICU patients.<sup>1,2</sup> Acute lung injury (ALI), the most common early complication of sepsis, presents as refractory hypoxemia and progressive dyspnea.<sup>3-5</sup> ALI affects 40% to 68.2% of adults with sepsis, significantly impacting both survival probabilities and the quality of life post-sepsis.<sup>3,6</sup> Current treatment of sepsis, including antibiotics, fluid

resuscitation, blood purification, mechanical ventilation, and multi-organ support often induce adverse reactions and reduce overall efficacy.<sup>7</sup> Therefore, timely, effective, and safe interventions are crucial for alleviating sepsis-related symptoms and improving patient survival and prognosis.

Recent clinical studies have shown that traditional Chinese medicine (TCM) offers significant clinical benefits and unique advantages as a complementary and alternative treatment for sepsis-induced acute lung injury (SALI).<sup>8,9</sup> Based on the clinical and pathological characteristics of SALI, Chinese medicine classifies it as “warm-heat disease”, “asthma syndrome”, or “dirty exhaustion”, among others. The underlying pathology of SALI is characterized by heat, toxicity, and stasis. Correspondingly, the therapeutic strategy encompasses several key aspects, including dispelling heat, detoxification, promoting blood circulation, resolving stagnation, and fortifying the body’s foundation.<sup>10–12</sup> Xijiao Dihuang Decoction (XJDHD), a formula from Sun Simiao’s pharmaceutical classic “Beiji Qianjin Yaofang”, is commonly used in Chinese medicine to treat sepsis. It is composed of buffalo horn (replacing rhinoceros horn), Rehmannia, White Paeony Root, and Cortex Moutan. Collectively, these herbs demonstrate heat-clearing, blood-cooling, detoxifying, and stasis-resolving properties, which are consistent with the pathogenesis of sepsis-induced acute lung injury (SALI).<sup>13</sup> Although prior research has examined the use of XJDHD in treating sepsis, the precise mechanism by which it treats SALI is still not well understood.<sup>14,15</sup> Moreover, most existing studies employ a single method which lacks an integrated approach.<sup>16</sup> Network pharmacology represents an emerging research methodology, distinguished by its systematic and holistic approach. It bears resemblance to the holistic principles and therapeutic strategies inherent in Traditional Chinese Medicine.<sup>17–19</sup> This study endeavors to elucidate the therapeutic mechanisms of XJDHD for SALI by integrating network pharmacology, molecular docking, molecular dynamics simulations, and in vitro cell experiments. Specifically, the objective is to ascertain whether XJDHD exerts its therapeutic effects on SALI via anti-inflammatory, antioxidant, and anti-apoptotic actions, along with the modulation of key signaling pathways, such as the PI3K/Akt pathway. This comprehensive approach is expected to deepen our understanding of the mechanisms underlying XJDHD’s efficacy and furnish a scientific foundation for future in vivo and clinical investigations.

## Information and Methods

### Prediction of Xijiao Dihuang Decoction’s Active Ingredients and Acquisition of Potential Targets

To identify the active chemical components of the four herbal medicines—Buffalo Horn, Rehmannia, White Paeony Root, and Cortex Moutan—in Xijiao Dihuang Decoction (XJDHD), we employed two databases: the Traditional Chinese Medicine Systems Pharmacology (TCMSP, accessible at <http://ibts.hkbu.edu.hk/LSP/tcmsp.php>) and the Herb Database (HERB, found at <http://herb.ac.cn/>).<sup>20,21</sup> In the screening for active ingredients, we set specific selection parameters: for chemicals sourced from the TCMSP, we considered those with an oral bioavailability (OB) of at least 30% and a drug-like property score (DL) of no less than 0.18. The criterion of  $OB \geq 30\%$  is a commonly used standard for screening compounds with good oral absorption, ensuring that the selected components achieve sufficient concentrations in the body to exert pharmacological effects.  $DL \geq 0.18$  is a commonly used standard for screening compounds with good drug-likeness, ensuring that the selected components can effectively bind to targets and exert pharmacological effects. Consequently, these two criteria were selected as the screening indicators for effective components in the TCMSP database.<sup>22</sup> As for the HERB database, we adhered to the Lipinski’s “Rule of Five” for inclusion. To predict and analyze the potential targets of these active ingredients within XJDHD, we leveraged the TCMSP’s database of related targets, along with the SwissTargetPrediction database (<http://www.swisstargetprediction.ch/>) and the PubChem database (<https://pubchem.ncbi.nlm.nih.gov/>).<sup>23,24</sup> Finally, the UniProt database was employed to convert the targets of XJDHD’s active ingredients into their corresponding standard gene names.<sup>25</sup>

### Collection of Disease-Related Targets

To identify disease-related targets pertinent to sepsis-induced acute lung injury, we utilized the GeneCards database (<https://www.genecards.org/>)<sup>26</sup> and the OMIM database (<https://www.omim.org/>) by conducting searches with the

keyword ‘sepsis-induced acute lung injury. The keyword was used to retrieve relevant data, which was then processed to obtain disease-related targets for sepsis-induced acute lung injury. To identify potential targets for the treatment of SALI, the jvenn platform (<http://jvenn.toulouse.inra.fr/>)<sup>27</sup> was employed to analyze the overlap between the active ingredient targets of XJDHD and the disease targets of SALI. Subsequently, a Venn diagram was generated to visually present the results of this analysis.

## Construction of the Traditional Chinese Medicine-Active Ingredient-Common Target Network Diagram

Using Cytoscape 3.9.1, a network visualization and analysis software, we constructed a network diagram that depicted the interconnections among “Traditional Chinese Medicine”, “Active Ingredients”, and “Common Targets”. The Degree value, a key network topology parameter, was subsequently analyzed through the Analyze Network plug-in to assess the significance of each node. Notably, a higher Degree value signifies greater prominence of a node. This critical parameter facilitated the identification of the most pertinent chemical components and targets associated with the active ingredients in XJDHD by filtering out those of lesser significance.

## PPI Network Construction for Xijiao Dihuang Decoction with SAL

The STRING database (<https://string-db.org>)<sup>28</sup> was utilized to import the common target proteins, with a filtering condition set to include only those with a combined score exceeding 0.4. After eliminating free targets, the data were then imported into Cytoscape 3.9.1 to construct a protein-protein interaction (PPI) network. The CytoHubba plug-in in Cytoscape 3.9.1 was employed to discern the top ten hub proteins of highest significance within this network.

## GO Functional Enrichment Analysis and KEGG Pathway Enrichment Analysis

To investigate the biological implications and functional significance of the protein targets involved in XJDHD’s therapeutic approach to treating SALI, GO enrichment and KEGG pathway enrichment analyses were conducted on these targets through the DAVID database (<https://david.ncicrf.gov/>)<sup>29</sup>, followed by visualization using the Microbiotics online tool (<http://www.bioinformatics.com.cn/>). This process aimed to uncover the underlying biological processes and pathways in which these targets are engaged.

## Molecular Docking

Following the identification of active ingredients and disease-related targets discussed in Section 1.3, nine primary target proteins in the protein-protein interaction network were selected for molecular docking analysis. Subsequently, leveraging the molecular docking outcomes, the protein-ligand complex exhibiting the optimal binding affinity was chosen. Through a comprehensive review of the relevant literature and in alignment with the objectives of this study, the known positive small-molecule drugs corresponding to the target protein were identified. Molecular docking was then carried out to establish the positive control group for the optimal-binding complex in this study. The two-dimensional structures of the drug ligands were obtained from the PubChem database (<http://pubchem.ncbi.nlm.nih.gov>) and optimized into their three-dimensional forms using Chem3D software through energy minimization processes. The crystal structures of the key target proteins were sourced from the Protein Data Bank (<https://www1.rcsb.org/>), with extraneous water molecules and ligands eliminated from the protein structures via PyMOL software. Thereafter, the protein receptor structures were hydrogen-optimized through AutoDock Tools 1.5.7, followed by converting the ligand and receptor formats, pinpointing the active binding sites. Ultimately, PyMOL software facilitated the visualization of molecular docking, depicting the spatial arrangement of the drug ligands attached to the core receptors and denoting the binding sites.

## Molecular Dynamics Simulation

In this study, Gromacs version 2022.3 software<sup>30,31</sup> was used to perform molecular dynamics simulations of Beta-Sitosterol in complex with AKT1/TNF. Small molecules were preprocessed with AmberTools22 and assigned the Generalized Amber Force Field (GAFF). Hydrogen atoms were added and RESP potentials computed using Gaussian

16W. For molecular dynamics simulations, the Amber99sb-ildn force field served as the foundation, with water molecules as the solvent environment, at a controlled temperature of 300 K and 1 bar pressure. To maintain electrical neutrality, an appropriate amount of Na<sup>+</sup> ions were incorporated to balance the system's total charge. The simulation protocol initiated with an energy minimization process, leveraging the steepest descent algorithm. Subsequently, distinct 100,000-step NVT and NPT equilibrations, each lasting 100 ps, were carried out with a coupling constant of 0.1 ps. Following this, unrestrained molecular dynamics simulations proceeded for 100 ns. Throughout the simulations, trajectory data were consistently recorded for subsequent analysis. The assessment of the molecular dynamics (MD) simulation results involved calculating several key parameters of the complexes, namely the root mean square deviation (RMSD), root mean square fluctuation (RMSF), radius of gyration (Rg), hydrogen bonding (H-bonds), and binding free energy (MMGBSA) of the complexes.

## Cellular Experimental Validation

### Experimental Animals and Cell Lines

In this study, A549 human type II alveolar epithelial cells (A549, procured from Saiku Bio) were utilized for the experiments.

### Drugs and Reagents

Xijiao Dihuang decoction is composed of Buffalo Horn (30 g, Cat: 2410142), Rehmannia (24 g, Cat: 2411059), White Peony Root (12 g, Cat: 2411138), and Cortex Moutan (9 g, Cat: 24051407). In this study, the Chinese herbal materials were obtained from the Chinese herbal pharmacy of the First Teaching Hospital of Tianjin University of TCM. They were authenticated by Wang Lei, Deputy Director of the Department of Pharmacy. The voucher specimens were stored in the Department of Pharmacy at the First Teaching Hospital of Tianjin University of TCM.

The following reagents were utilized in this study:

DMEM basal medium (GIBCO, USA, batch no. 12491015); penicillin and streptomycin (GIBCO, USA, batch no. 15140148); fetal bovine serum (Clark, batch no. FB15011); lipopolysaccharide (Sigma, USA, batch no. L2630); CCK-8 cell viability assay kit (Abmole, batch no. CK001); The ELISA kits for IL-6 (batch no. ml038115), TNF- $\alpha$  (batch no. ml077385) and IL-1 $\beta$  (batch no. ml058059) produced by Shanghai Enzyme-Link Bio-Technology Co; TRIzol reagent (Invitrogen, USA, batch no. 15596018CN); PrimeScript RT kit (Takara, Japan, batch no. RR037A); SYBR Green Master Mix (Applied Biosystems, USA, batch no. A25742); Anti-GAPDH antibody [6C5] (abcam, lot no. ab8245); Recombinant Anti-Bax antibody [E63] (abcam, lot no. ab32503); Recombinant Anti-Bcl-2 antibody [EPR17509] (abcam, lot no. ab182858); Recombinant Anti-Cleaved Caspase-3 antibody [E83-77] (abcam, lot no. ab32042); Phospho-Akt (Ser473) (CST, lot no. 4060T); Phospho-PI3 Kinase p85 (Tyr458) (CST, lot no. 17366T).

## Instrumentation

### The Following Instruments Were Utilized in This Study

Fluorescence quantitative PCR system (Applied Biosystems, Inc., USA); carbon dioxide cell culture incubator (Thermo, Inc., USA); ultra-clean bench (Suzhou Antai Science and Technology Co., Ltd.); high-speed tabletop centrifuge (Anhui Zhongke Zhongjia Scientific Instrument Co., Ltd.); constant temperature water bath (CU600, Shanghai Yihang Co., Ltd.); ultra-low-temperature freezer (Qingdao Haier Co., Ltd.); Enzyme Labeling Instrument (Bio-Tek, USA); and Western Blot Developer (Shanghai Tanon Technology Co., Ltd).

### Preparation of Xijiao Dihuang Decoction Lyophilized Powder

To prepare Xijiao Dihuang Decoction, the formula included Buffalo Horn (30 grams), Rehmannia (24 grams), White Peony Root (12 grams), and Cortex Moutan (9 grams), all at a 10-fold dosage. Initially, the raw herbs were soaked in 10 times their volume of pure water for 30 minutes, then boiled and decocted for 60 minutes to extract the essence. Subsequently, 8 times the volume of water was added to the residue, which was then boiled for an additional 30 minutes. The combined filtrates were collected. Condensed, freeze-dried powder, corresponding to an extraction yield of 31.47%. The obtained powder was portioned and stored at  $-80^{\circ}\text{C}$ . Prior to administration, the drug was diluted to various concentrations and filtered through a 0.22  $\mu\text{m}$  filter.

### CCK8 Assay for Cell Proliferative Activity

To evaluate the effect on cell proliferation, A549 cells were initially seeded at a density of  $2 \times 10^4$  cells/well in 96-well plates. Once the cells had adhered to the plate, they were treated with differing concentrations of Xijiao Dihuang decoction lyophilized powder (0, 50, 100, 200, 400, 800, and 1000  $\mu\text{g/mL}$ ). Following an incubation period of 24 hours in a  $37^\circ\text{C}$ , 5%  $\text{CO}_2$  incubator, 10  $\mu\text{L}$  of CCK8 reagent was introduced to each well and the mixture was allowed to incubate for a further 2 hours. Subsequently, the absorbance at 450 nm was measured and used to calculate the cell proliferation inhibition rate. The entire procedure was repeated in triplicate for consistency.

### Culture and Grouping of Human Type II Alveolar Epithelial A549 Cells

A549 human type II alveolar epithelial cells were cultured in Dulbecco's Modified Eagle's Medium (DMEM) supplemented with 10% fetal bovine serum, 100 U/mL penicillin, and 100  $\mu\text{g/mL}$  streptomycin. The cells were cultured at  $37^\circ\text{C}$  in an atmosphere containing 5%  $\text{CO}_2$ . When the cells reached the logarithmic growth phase, 30  $\mu\text{g/mL}$  LPS was selected as the treatment concentration to establish the A549 cell inflammation model, based on preliminary experiments ([Supplementary Figure 1](#)). Based on the experimental results presented in Section 2.8.1, it was determined that 100  $\mu\text{g/mL}$  and 200  $\mu\text{g/mL}$  of XJDHD exerted no significant influence on cell viability within a 24-hour period. This finding ensured the safety and efficacy of the experiment. As a result, 100  $\mu\text{g/mL}$  and 200  $\mu\text{g/mL}$  of XJDHD were chosen as the low (XJDHD-L) and high (XJDHD-H) dose intervention concentrations of XJDHD. Therefore, the cells were divided into four experimental groups: a Control group, which received DMEM with 10% serum; a Model group, which was exposed to 30  $\mu\text{g/mL}$  lipopolysaccharide (LPS) and 10% serum; an XJDH-L group, which was treated with 30  $\mu\text{g/mL}$  LPS, 10% serum, and 100  $\mu\text{g/mL}$  of XJDHD; and an XJDH-H group, which was exposed to 30  $\mu\text{g/mL}$  LPS, 10% serum, and 200  $\mu\text{g/mL}$  of XJDHD.

### ELISA Assay for IL-6, IL-1 $\beta$ , and TNF- $\alpha$ in Cells

The levels of IL-6, IL-1 $\beta$ , and TNF- $\alpha$  in the supernatants collected from each group of A549 cells were determined. The enzyme-linked immunosorbent assay (ELISA) kit protocol was strictly followed for accurate measurement of the cytokine concentrations.

### q-PCR Assay for SOD, MyD88, and CAT-Related RNA in Cells

A549 cells were harvested, and total RNA was extracted from these cells using Trizol reagent. Subsequently, reverse transcription was conducted to synthesize cDNA. For the quantification PCR analysis, cDNA was amplified with the aid of SYBR Green PCR Master Mix. The qPCR protocol included an initial denaturation step at  $95^\circ\text{C}$  for 30 seconds, followed by 40 cycles consisting of 10 seconds at  $95^\circ\text{C}$  for denaturation, 20 seconds at  $58^\circ\text{C}$  for annealing, and 30 seconds at  $72^\circ\text{C}$  for extension. To ensure data accuracy, GAPDH was employed as the internal reference for normalization, and each sample underwent three technical replicates. The primer details are provided in the [Table 1](#).

### Western Blot Assay for p-Akt, p-PI3K, BCL-2, Bax, and C-Caspase 3 Proteins in Cells

To investigate the expression levels of p-AKT, p-PI3K, BCL-2, Bax, and C-Caspase 3 proteins in different experimental groups of A549 cells, Western Blot analysis was performed. Proteins were extracted from cells collected from each group

**Table 1** Primer Sequences

Gene Name	Primer Sequences (5'-3')	Product Length/bp
MyD88	F: AGAGCTGCTGGCCTTGTTAG R: CGAAAAGTTCGGCGTTTGT	168
SOD	F: GGAAGCATGGCGATGAAAGC R: CCCCATACTGATGGACGTGG	167
CAT	F: AAGATTGCCTTCTCCGGGTG R: GACCCCGCGGTCATGATATT	227
GAPDH	F: AATGGGCAGCCGTTAGGAAA R: GCGCCCAATACGACCAAATC	168

using RIPA lysis buffer, and their concentration was assessed through the BCA method. After standardizing the concentrations, equal quantities of proteins, based on molecular weight, were separated by SDS-PAGE gel electrophoresis for 1 hour. Subsequently, proteins were transferred to PVDF membranes through wet transfer. These membranes were then blocked with 5% skimmed milk for 1 hour prior to being incubated with primary antibodies at 4°C overnight. The employed primary antibodies included: Anti-p-Akt Rabbit mAb (1:2000), Anti-p-PI3K Rabbit mAb (1:1000), Anti-cleaved Caspase-3 Rabbit mAb (1:1000), Anti-Bcl-2 Rabbit mAb (1:2000), Anti-Bax Rabbit mAb (1:1000), and Anti-GAPDH Mouse mAb (1:2000). Following this, the membranes were incubated with a secondary antibody (1:2000) in 5% skim milk for another hour. Protein bands were visualized using an HRP chemiluminescent substrate, and their intensity was quantitatively analyzed with ImageJ software.

## Statistical Methods

The experiments were performed in triplicate to guarantee the stability and reproducibility of the results. All experimental data were analyzed statistically using SPSS 22.0 software and graphed using GraphPad Prism 10.0 software. The normality of the data was evaluated via the Shapiro–Wilk test. Data are presented as mean  $\pm$  standard deviation. Subsequently, the homogeneity of variances was evaluated using Levene’s test. In the event that the variances were homogeneous, a one-way analysis of variance (ANOVA) was conducted, and this was succeeded by Tukey’s multiple comparisons test for multiple-group comparisons. A *P*-value of less than 0.05 was regarded as indicating statistical significance.

## Results

### Screening of Chemical Compositions and Action Targets of Chinese Medicines

A search for the chemical components of the four herbs in XJDHD was conducted in the TCMSP and HERB databases, revealing 195 putatively active compounds. We applied different screening methods for different herbs in XJDHD. For White Paeony Root and Cortex Moutan, a screening process was carried out with an oral bioavailability (OB) threshold of 30% and a drug-likeness (DL) score of at least 0.18. As a result, a total of 24 active ingredients were identified in these two herbs, including 13 from White Paeony Root and 11 from Cortex Moutan. Regarding Buffalo Horn and Rehmannia, they were screened according to Lipinski’s “Rule of Five”. This screening led to the identification of 11 active ingredients, with 5 from Buffalo Horn and 6 from Rehmannia. The effective components of White Paeony Root and Cortex Moutan were predicted by means of the Related Targets tool in the TCMSP database. The active chemical components of Buffalo Horn and Rehmannia were retrieved from the PubChem database, from which their SMILES representations were obtained. These SMILES notations were then utilized for target prediction in the SwissTargetPrediction database. After standardization and de-emphasis processes in the UniProt database, a total of 313 gene targets were identified. Additionally, 35 active ingredients in XJDHD were identified, of which 11 failed to match the corresponding targets. After the removal of duplicates, 20 active ingredients were retained (Table 2 and Table 3).

**Table 2** Identification of Active Constituents in XJDHD via the TCMSP Database

ID	Molecule Name (Drug)	OB/%	DL
DP1	Quercetin (Cortex Moutan)	46.43	0.28
DP2	5-[[5-(4-methoxyphenyl)-2-furyl]methylene]barbituric acid (Cortex Moutan)	43.44	0.3
DP3	Mairin (Cortex Moutan, White Paeony Root)	55.38	0.78
DP4	Sitosterol (Cortex Moutan, White Paeony Root)	36.91	0.75
DP5	Kaempferol (Cortex Moutan, White Paeony Root)	41.88	0.24
DP6	(+)-catechin (Cortex Moutan, White Paeony Root)	54.83	0.24

(Continued)

**Table 2** (Continued).

ID	Molecule Name (Drug)	OB/%	DL
BS1	Beta-sitosterol (White Paeony Root)	36.91	0.75
BS2	Paeoniflorgenone (White Paeony Root)	87.59	0.37
BS3	(3S,5R,8R,9R,10S,14S)-3,17-dihydroxy-4,4,8,10,14-pentamethyl-2,3,5,6,7,9-hexahydro-1H-cyclopenta[a]phenanthrene-15,16-dione (White Paeony Root)	43.56	0.53
BS4	Paeoniflorin (White Paeony Root)	53.87	0.79

**Abbreviations:** XJDHD, Xijiao Dihuang decoction; OB, oral bioavailability; DL, drug-likeness.

**Table 3** Identification of Active Constituents in XJDHD via the HERB Database

ID	Molecule Name (Drug)	Wm/ (g-mol-1)	Alogp/a <sup>2</sup>	Hdon	Hacc
SNJ1	Arginine (Buffalo Horn)	174.2	-4.2	4	4
SNJ2	Alanine (Buffalo Horn)	89.09	-3	2	3
SNJ3	Aspartic acid (Buffalo Horn)	133.1	-2.8	3	5
SNJ4	4-Guanidino-1-butanol (Buffalo Horn)	131.18	-1.3	3	2
SD1	Adenosine (Rehmannia)	267.24	-1.1	4	8
SD2	Uridine (Rehmannia)	244.2	-2	4	6
SD3	Rehmaglutin c (Rehmannia)	200.19	-2.5	3	5
SD4	Guanosine (Rehmannia)	283.24	-1.9	5	7
SD5	Salidroside (Rehmannia)	300.3	-0.6	5	7
SD6	Coniferin (Rehmannia)	314.38	-1.3	5	8

**Abbreviations:** XJDHD, Xijiao Dihuang decoction; MW, Molecular Weight; ALogP, octanol/water partition coefficient; Hdon, number of Hydrogen Bond Donors; Hacc, number of Hydrogen Bond Acceptors.

## Disease Target Screening

Initially, a total of 547 SALI gene targets were retrieved from the Online Mendelian Inheritance in Man (OMIM) database. This number was further expanded to 2,752 targets when data was extracted from the GeneCards database. After consolidating these datasets and eliminating duplicates, a cumulative list of 3,250 unique targets was obtained. To visualize the overlap between the targets affected by Chinese medicine and those associated with the disease, the Jvenn platform was employed to construct a Venn diagram (Figure 1). This diagram elucidated the intersecting genes targeted by both the Chinese medicine and the disease through the analysis. As a result, 182 potential targets were identified for the action of XJDHD in treating SALI, along with 17 effective chemical components.

## Traditional Chinese Medicine-Active Ingredient-Common Target Networks

The chemical constituents of Chinese medicines and their corresponding common target genes were imported into Cytoscape 3.9.1 software, which enabled the visualization of the “Chinese medicines-active ingredients-common targets” network, as depicted in Figure 2. The top 9 active ingredients were identified as being quercetin, kaempferol, salidroside, adenosine, guanosine, rehmaglutin C, beta-sitosterol, uridine, and (+)-catechin. The specific topological parameters are presented in Table 4.

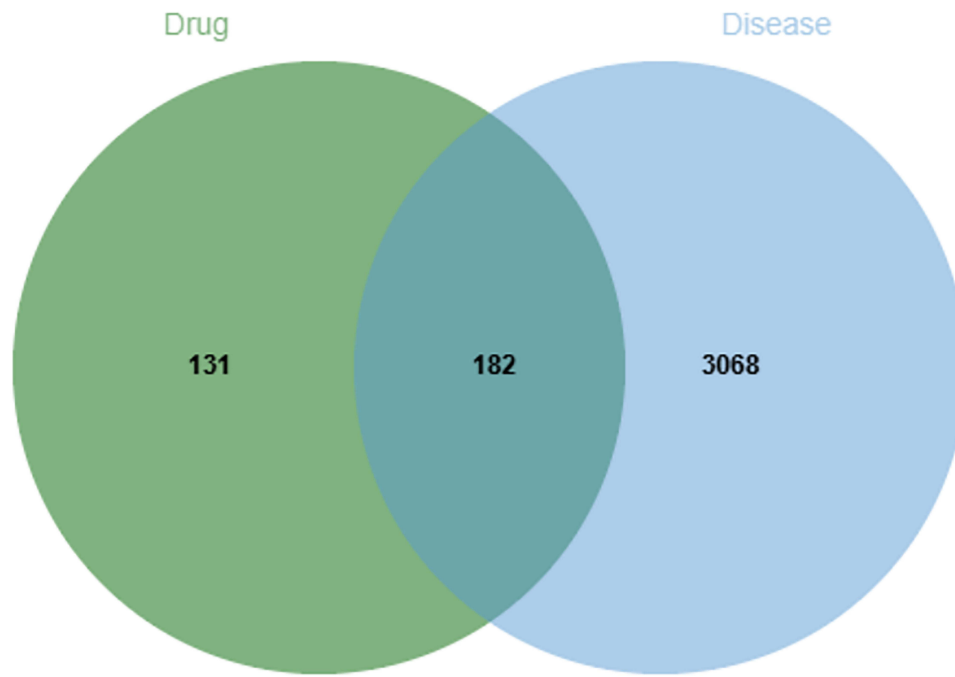


**Figure 1** Venn diagram of intersecting targets of XJDHD for the treatment of SALI.

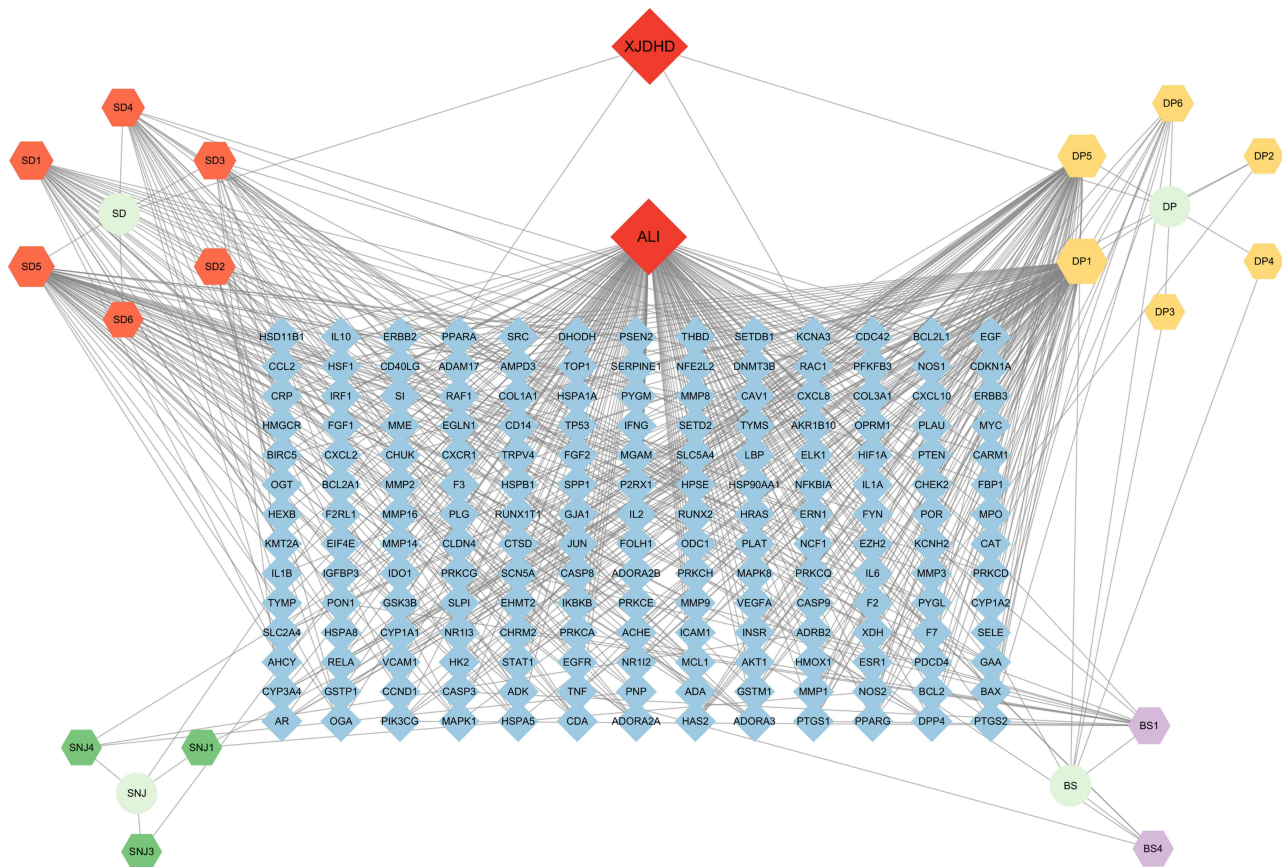


**Figure 2** Traditional Chinese Medicine-Active Ingredient-Common Target Network of XJDHD for the Treatment of SALI.

**Table 4** The Main Active Ingredient in XJDHD for the Treatment of SALI

ID	Molecule Name	Degree Centrality	Betweenness Centrality	Closeness Centrality
DP1	Quercetin	101	0.148 564 253	0.51
DP5	Kaempferol	76	0.028 355 218	0.389 312 977
SD5	Salidroside	54	0.042 952 711	0.408
SD1	Adenosine	31	0.013 415 327	0.372 262 774
SD4	Guanosine	25	0.007 857 41	0.364 285 714
SD3	Rehmaglutinin c	21	0.008 165 716	0.361 702 128
BS1	Beta-sitosterol	16	0.005 973 142	0.352 941 176
SD2	Uridine	13	0.002 666 407	0.348 122 867
DP6	(+)-catechin	12	0.002 109 766	0.342 281 879

**Abbreviations:** XJDHD, Xijiao Dihuang decoction; SALI, Sepsis-Induced Acute Lung Injury.

### PPI Network Construction and Core Target Extraction

Based on the previous identification of 182 potential targets for XJDHD in treating SALI, the 182 common gene targets of XJDHD and SALI were imported into the STRING database, with the species restricted to “Homo sapiens.” Potential targets with a minimum required interaction score greater than 0.4 were selected. The resulting data were imported into Cytoscape 3.9.1 for visual analysis, and the PPI network was constructed, as shown in Figure 3A. A total of 180 nodes and 3573 edges were obtained. Using the CytoHubba plugin in Cytoscape 3.9.1, the centrality scores were calculated based on the MCC algorithm. Subsequently, the top 20 hub proteins (Figure 3B and Table 5) and the top 10 hub proteins (Figure 3C) were identified. The top 10 hub proteins are as follows: IL6, TNF, AKT1, MMP9, HIF1A, JUN, BCL2, PTGS2, IL1B, and CASP3. These ten targets are considered the core targets of XJDHD in treating SALI.

### GO Function and KEGG Analysis

To analyze the therapeutic mechanisms of XJDHD in treating SALI, the 182 overlapping targets derived from the intersection of Chinese medicine gene targets and disease gene targets were inputted into the DAVID database. Annotated

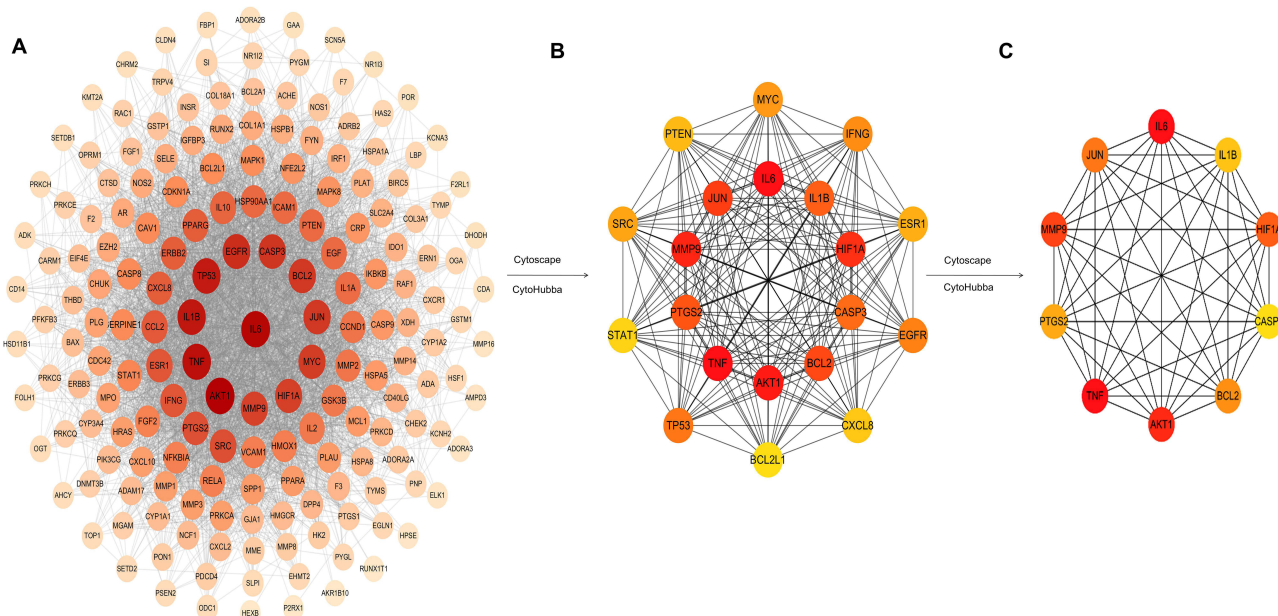


**Figure 3** PPI network and core targets of XJDHD for SALI treatment.(A)PPI network; (B) Top 20 hub proteins(As the color becomes darker, the ranking increases. Conversely, if the color becomes lighter, the ranking decreases); (C) Top 10 hub proteins(As the color becomes darker, the ranking increases. Conversely, if the color becomes lighter, the ranking decreases).

**Table 5** Top 20 Proteins in the Network Ranked by the MCC Method

Rank	Name	Score	Rank	Name	Score
1	TNF	1.91524190903048×10 <sup>39</sup>	11	TP53	1.91524190774395×10 <sup>39</sup>
1	IL6	1.91524190903048×10 <sup>39</sup>	12	EGFR	1.91524190761841×10 <sup>39</sup>
3	AKT1	1.91524190903041×10 <sup>39</sup>	13	IFNG	1.91524189791625×10 <sup>39</sup>
4	MMP9	1.91524190903038×10 <sup>39</sup>	14	MYC	1.91524179731859×10 <sup>39</sup>
5	HIF1A	1.91524190902965×10 <sup>39</sup>	15	SRC	1.91524173417137×10 <sup>39</sup>
6	JUN	1.9152419090291×10 <sup>39</sup>	16	ESR1	1.91524073686808×10 <sup>39</sup>
7	BCL2	1.91524190896299×10 <sup>39</sup>	17	PTEN	1.9152400056686×10 <sup>39</sup>
8	PTGS2	1.91524190870274×10 <sup>39</sup>	18	CXCL8	1.91523922636537×10 <sup>39</sup>
9	IL1B	1.91524190868907×10 <sup>39</sup>	19	STAT1	1.91521920886644×10 <sup>39</sup>
10	CASP3	1.91524190841981×10 <sup>39</sup>	20	BCL2	1.91520144359306×10 <sup>39</sup>

**Abbreviations:** MCC, (Maximum Clique Centrality): Identifying nodes with centrality in the maximum clique.

with a significance threshold of P-value < 0.05, 51 Gene Ontology (GO) enrichment terms emerged: 22 Biological Processes (BPs), 19 Molecular Functions (MFs), and 7 Cellular Components (CCs). The top 10 terms from each GO category were chosen for visualization (Figure 4 and Supplementary Table 1). The biological process enrichment analysis highlighted that essential processes involved in XJDHD’s efficacy for SALI treatment encompass host-virus interaction, apoptosis, inflammatory response, regulation of biological rhythms, chemotaxis, hemostasis, collagen degradation, blood coagulation, glycogen metabolism, and fibrinolysis.

A total of 165 signaling pathways (p < 0.05) were identified through KEGG pathway enrichment analysis. Subsequently, the focus was placed on the top 20 pathways for visualization and representation in a bubble map (Figure 5 and Supplementary Table 2). Notably, these pathways encompassed significant biological processes such as the MAPK signaling pathway, the PI3K-Akt signaling pathway, HIF-1 signaling pathway, IL-17 signaling pathway, TNF signaling pathway, and Kaposi sarcoma-associated herpesvirus infection pathway.

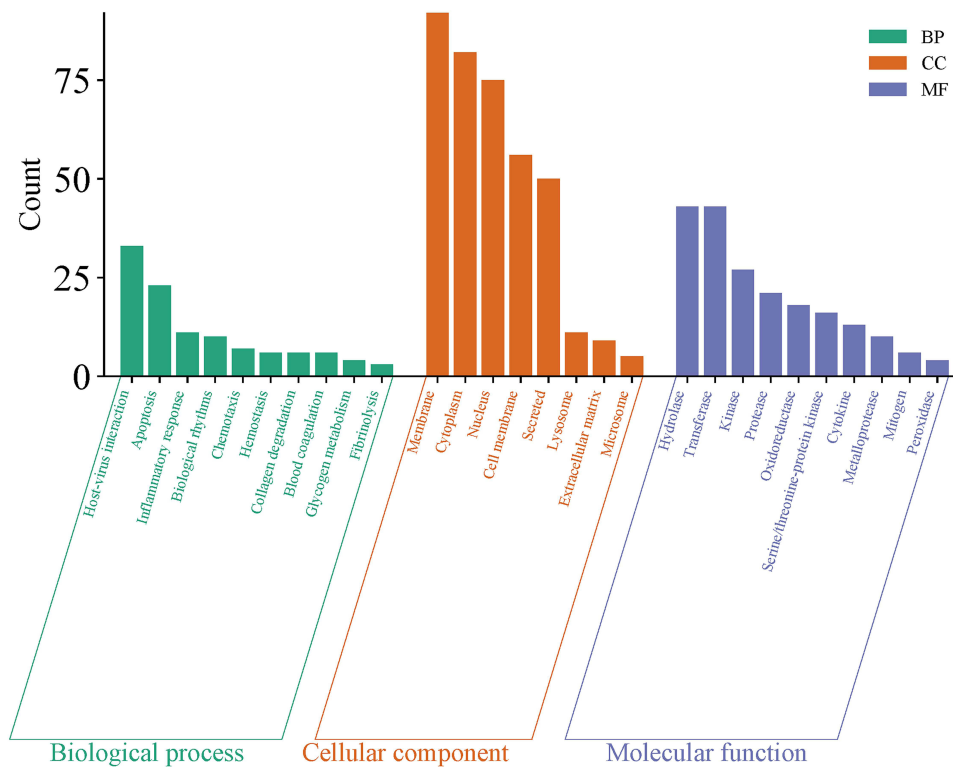


**Figure 4** GO functional enrichment analysis.(The top 10 items of each section are displayed in a bar chart with a selection criterion of p < 0.05.).

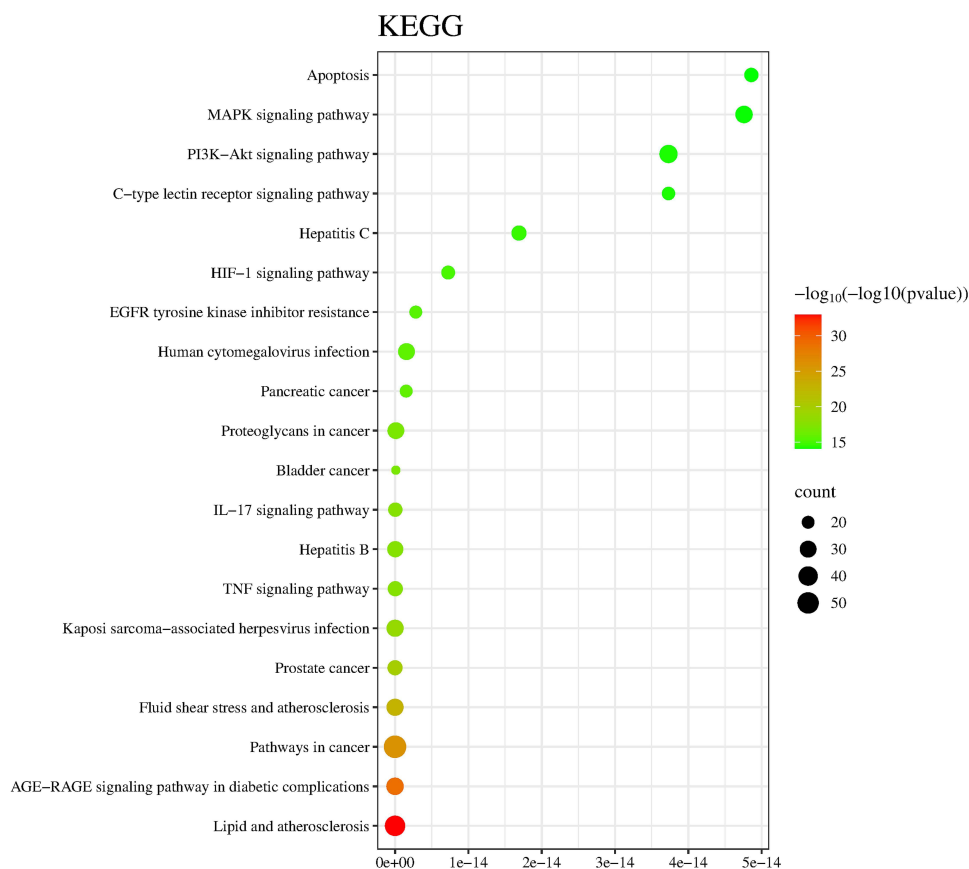


**Figure 5** KEGG pathway enrichment analysis.(The top 20 pathways are displayed in a bubble chart based on a selection criterion of  $p < 0.05$ .The bubble size indicates the number of genes enriched by the pathway; the redder the bubble color, the greater the corrected P-value and the greater the enrichment significance.).

To further explore the relationships among active ingredients, targets, and pathways involved in the therapeutic effects of XJDHD on SALI, an “Active Ingredients–Targets–Pathways” network diagram was generated using Cytoscape 3.9.1 (Figure 6). The network consists of 143 nodes and 808 edges, including 12 active ingredients, 20 signaling pathways, and 109 targets. The Degree value, a network topology parameter, was subsequently computed using the Analyze Network plugin. A higher Degree value reflects a node’s greater importance. The results reveal that the top five ranked targets (Table 6) include MAPK1, AKT1, RELA, IKBKB, and CHUK. The primary active ingredients (Table 7) include quercetin, kaempferol, salidroside, guanosine, and rehmaglutin C, whereas the key pathways (Table 8) consist of Pathways in Cancer, Lipid and Atherosclerosis, PI3K–Akt Signaling Pathway, MAPK Signaling Pathway, and AGE–RAGE Signaling Pathway in Diabetic Complications. These findings imply that XJDHD could exert therapeutic effects on SALI through multiple ingredients, multiple pathways, and multiple targets.

## Molecular Docking

Molecular docking techniques were employed in the analysis of the top nine core target proteins in the PPI network (IL6, TNF, AKT1, MMP9, HIF1A, BCL2, PTGS2, IL1B, CASP3) and the top nine core components of XJDHD (salidroside, quercetin, kaempferol, adenosine, guanosine, rehmaglutin c, beta-sitosterol, uridine, (+)-catechin). In molecular docking, a binding energy of  $\leq -5.0$  kcal/mol serves as an indicator that the active ingredients of the traditional Chinese medicine were well bound to the target proteins. Moreover, lower binding energies are associated with more stable and stronger binding structures. As depicted in Figures 7 and Supplementary Table 3, the molecular docking outcomes demonstrated that the binding affinity of Beta-Sitosterol to AKT1 and TNF was optimal, with binding energies of  $-11.31$  kcal/mol and  $-9.49$  kcal/mol, respectively. Additionally, apart from the binding energy of  $-4.9$  kcal/mol between JUN and rehmaglutin c, the lowest binding energies of

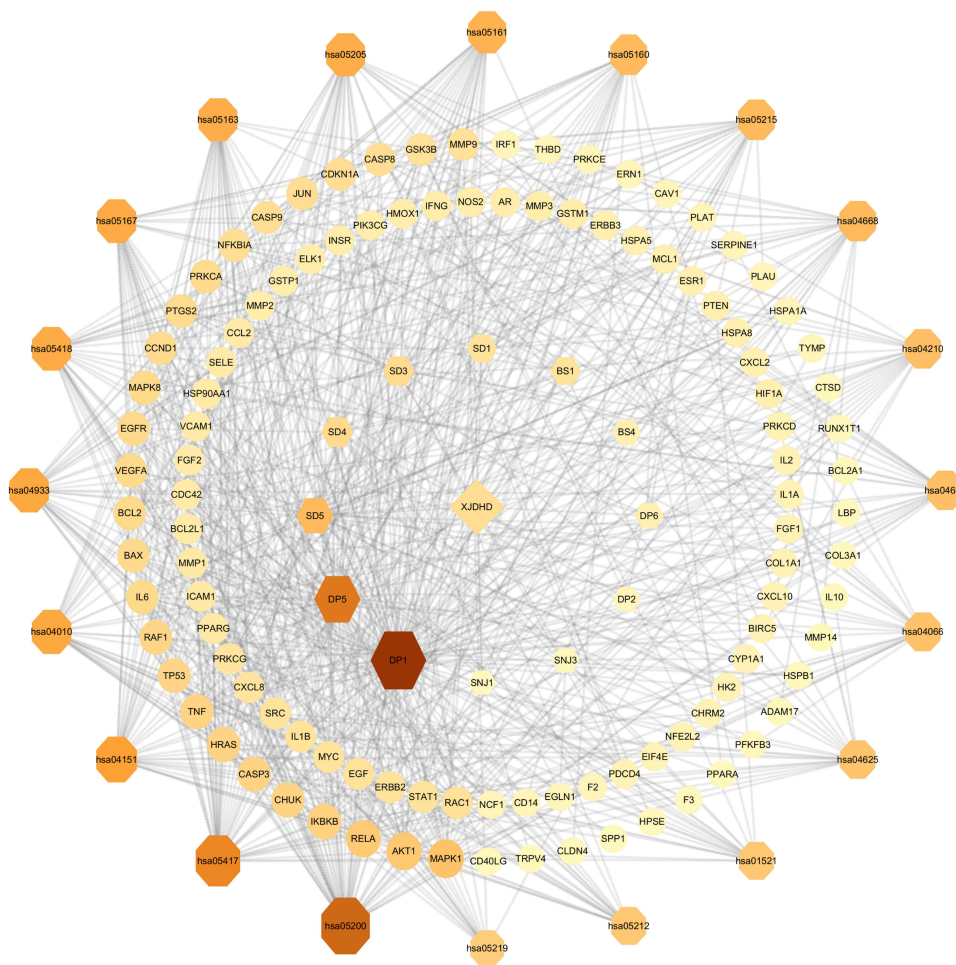


**Figure 6** Component-target-pathway network.(Ellipses represent targets, hexagons represent components, and octagons represent pathways. Node size and color intensity indicate degree ranking and importance: larger, darker nodes represent higher rankings and greater importance).

the remaining active components to their target proteins were all less than  $-5.0$  kcal/mol. These findings suggest that the key active ingredients of XJDHD establish a more robust and stable interaction with the core target proteins.

Additionally, to further validate whether beta-sitosterol can act as a potential active agent for AKT1 and TNF, relevant research results were reviewed,<sup>32,33</sup> and the well-established positive small-molecule drugs SC79 for AKT1 and SPD304 for TNF were chosen as positive controls for molecular docking. Molecular docking was performed independently for these positive control drugs. The binding energies obtained were  $-11.15$  kcal/mol for SC79-AKT1 and  $-9.27$  kcal/mol for SPD304-TNF ([Supplementary Figure 2](#)). Thus, it can be inferred that the binding affinity of  $\beta$ -sitosterol with

**Table 6** Topological Features of Core Components in the Active Ingredient-Target-Pathway Network

Rank	Target	DC	BC	CC
1	MAPK1	23	0.031	0.520
2	AKT1	21	0.017	0.511
3	RELA	20	0.015	0.500
4	IKBKB	17	0.008	0.470
5	CHUK	16	0.009	0.483

**Abbreviations:** DC, Degree Centrality; BC, Betweenness Centrality; CC, Closeness Centrality.

**Table 7** Topological Features of Core Components in the Active Ingredient-Target-Pathway Network

Rank	Molecule name	ID	DC	BC	CC
1	Quercetin	DPI	76	0.267	0.583
2	Kaempferol	DP5	51	0.025	0.412
3	Salidroside	SD5	26	0.057	0.415
4	Guanosine	SD4	14	0.013	0.387
5	Rehmaglutin c	SD3	13	0.013	0.379

**Abbreviations:** DC, Degree Centrality; BC, Betweenness Centrality; CC, Closeness Centrality.

**Table 8** Topological Features of Core Pathways in the Active Ingredient-Target-Pathway Network

Rank	Pathway	ID	DC	BC	CC
1	Pathways in cancer	hsa05200	57	0.118	0.507
2	Lipid and atherosclerosis	hsa05417	46	0.085	0.461
3	PI3K-Akt signaling pathway	hsa04151	36	0.045	0.433
4	MAPK signaling pathway	hsa04010	33	0.037	0.422
5	AGE-RAGE signaling pathway in diabetic complications	hsa04933	33	0.041	0.422

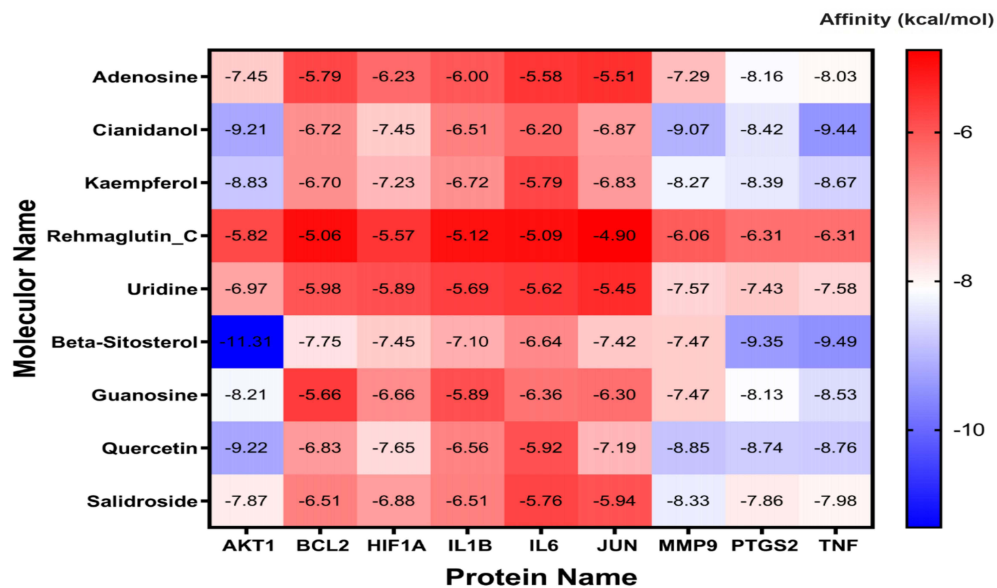
**Abbreviations:** DC, Degree Centrality; BC, Betweenness Centrality; CC, Closeness Centrality.

AKT1 and TNF is comparable to that of the known positive small-molecule drugs. This further validates that  $\beta$ -sitosterol may be a potential active drug targeting AKT1 and TNF.

## Molecular Dynamics Simulations

Based on the findings from Section 2.6, two targets with better docking affinities for Beta-Sitosterol were selected, and the Beta-Sitosterol-AKT1/TNF complex was analyzed via a 100 ns MD simulation. From the simulation trajectory data, the RMSD, RMSF, Rg, hydrogen bonds (H-bonds), and MMGBSA were calculated, as shown in Figures 8 and 9. RMSD is an index for evaluating the structural changes of protein-ligand complexes. A smaller RMSD indicates less significant the structural changes, suggesting greater stability of the complexes. As shown in Figure 8A, the RMSD curve of the Beta-Sitosterol-AKT1 complex stabilizes after approximately 20 ns, fluctuating between 0.15 and 0.25 nm. In contrast, the RMSD curve of the Beta-Sitosterol-TNF complex stabilizes after approximately 35 ns, fluctuating between 0.20 and 0.35 nm. The results indicate that the stability of the Beta-Sitosterol-TNF complex is slightly lower; however, the fluctuation ranges of both the Beta-Sitosterol-AKT1 and Beta-Sitosterol-TNF complexes are within 1 nm, suggesting that Beta-Sitosterol forms a stable complex with both AKT1 and TNF. RMSF is an indicator used to assess the dynamics of proteins. A higher RMSF value indicates greater fluctuation of amino acid residues, while a lower RMSF value corresponds to less fluctuation. In Figure 8B, the amino acid residues of AKT1 exhibit greater flexibility in the ranges of 180–190, 300–310, and 350–360, while those of TNF exhibit greater flexibility in the ranges of 70–75, 80–90, and 100–110. The radius of gyration (Rg) reflects a molecule's volume and compactness; smaller Rg values correspond to a more compact molecular arrangement, whereas larger Rg readings imply a more extended structure. In Figure 8C, The Beta-Sitosterol-AKT1 complex oscillates between 2.00 and 2.10, while the Beta-Sitosterol-TNF complex stabilizes between 2.15 and 2.20. To assess the structural stability of the complex, the Gibbs free energy landscape was employed. This landscape was characterized using RMSD and Rg metrics, as depicted in Figure 9A and B. In this landscape, blue and purple regions indicate lower free energy areas, typically corresponding to more thermodynamically stable conformations, while red regions represent higher free energy areas, usually associated with less stable conformations. The Beta-Sitosterol-AKT1 complex attains its most stable conformation when its Rg value is between 1.95 and 1.99 nm, with the free energy reaching its minimum and the RMSD value between 0.44 and 0.45 nm. Similarly, the Beta-Sitosterol-TNF complex achieves its most stable conformation when their Rg values range from 2.17 to 2.18 nm. At this state, the

**A**



**B**

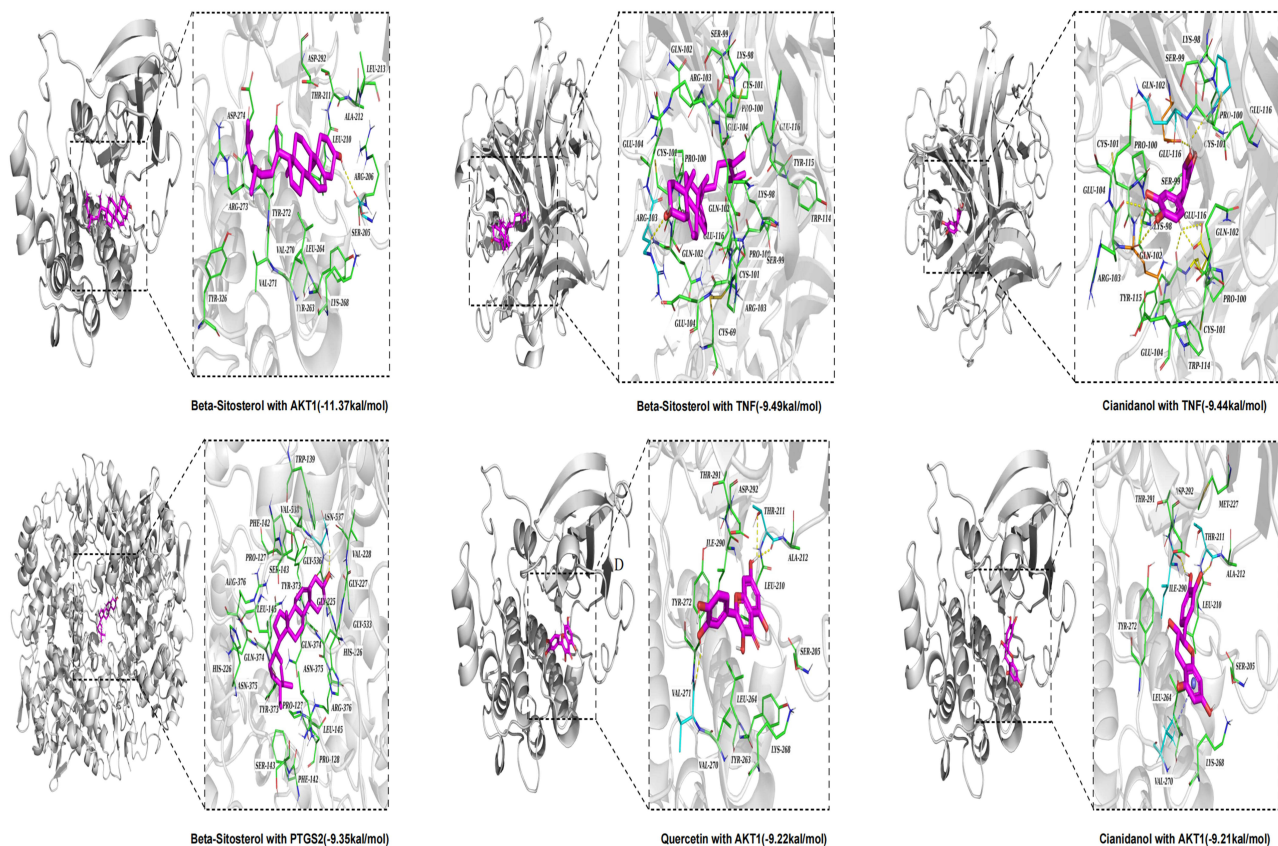


**Figure 7** Molecular docking analysis. **(A)** The molecular docking binding energy between the 9 active components and the 9 core targets(The colors in the heatmap are encoded based on the binding affinity values between compounds and targets, with the specific color gradient indicated in the color bar within the figure.); **(B)** The results of molecular docking.

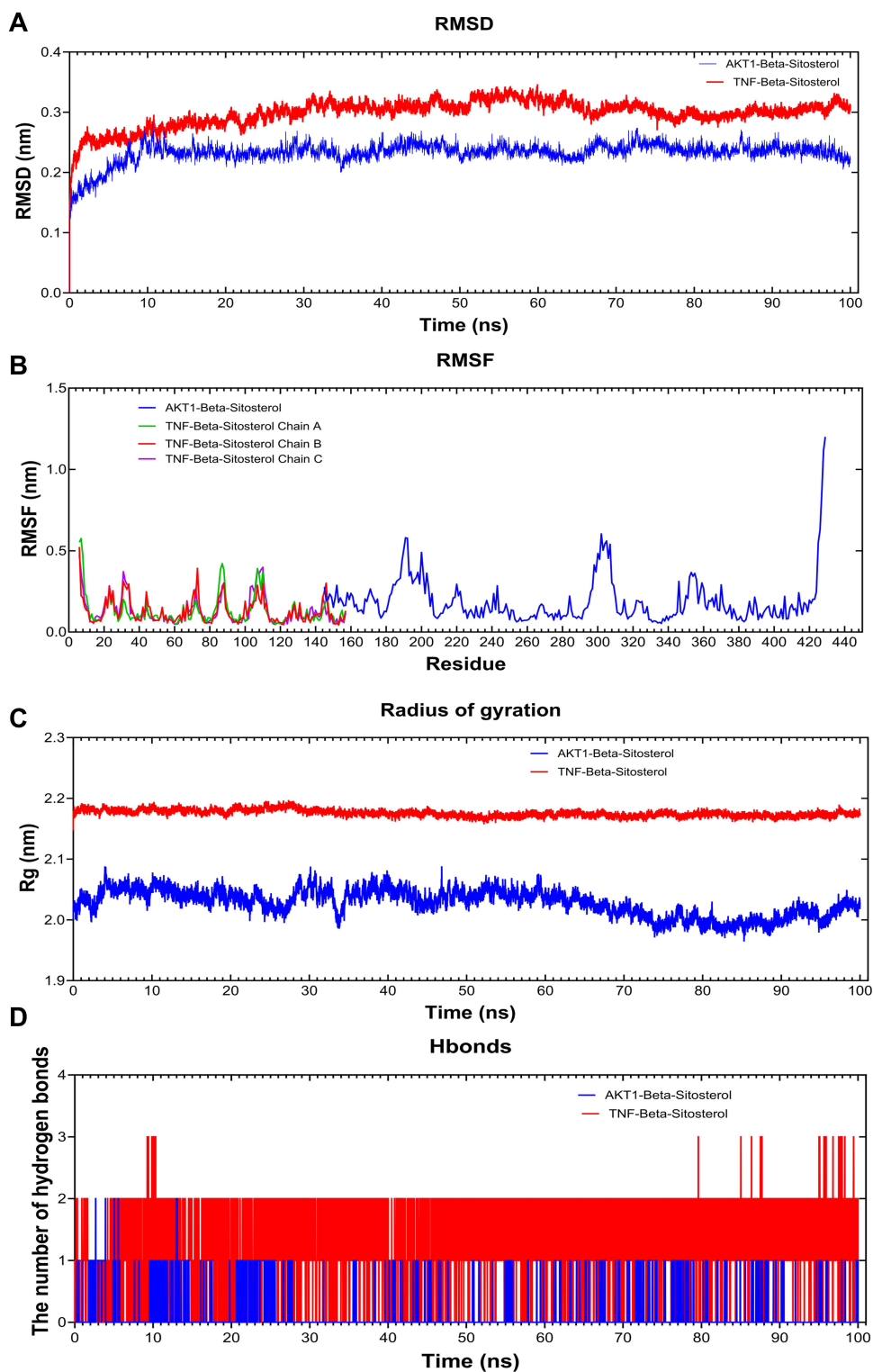


**Figure 8** Molecular dynamics simulation of beta-sitosterol-AKT1, beta-sitosterol-TNF: (A): RMSD curves of beta-sitosterol-AKT1/TNF complexes; (B): RMSF curve of beta-sitosterol-AKT1/TNF complexes; (C): Rg curves of beta-sitosterol-AKT1/TNF complexes; (D): Number of hydrogen bonds in the beta-sitosterol-AKT1/TNF complexes.

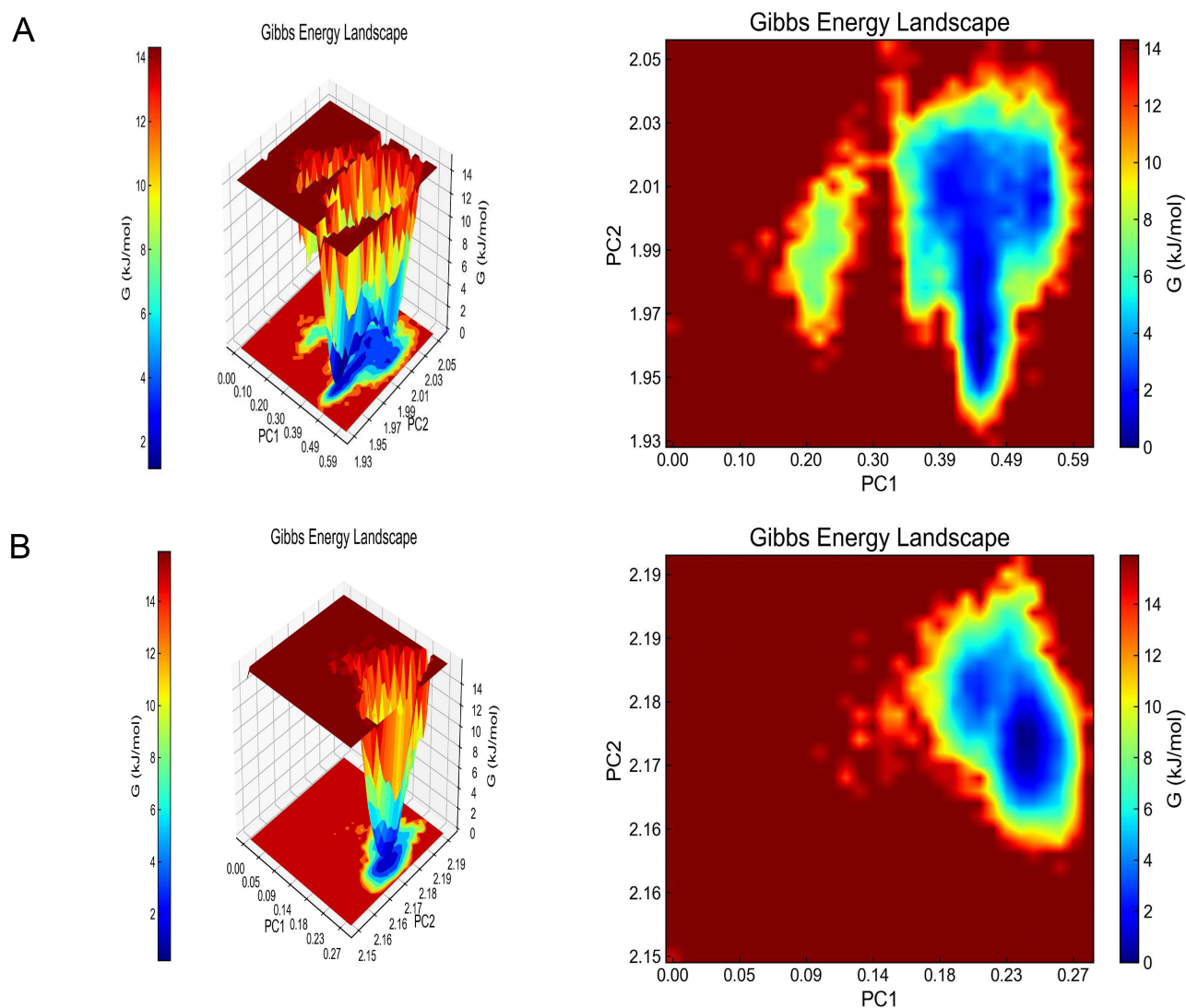


**Figure 9** Gibbs free energy analysis results. **(A)**: Beta-Sitosterol-AKT1; **(B)**: Beta-Sitosterol-TNF.

free energy is minimized, with RMSD values between 0.24 and 0.25 nm. In [Figure 8D](#), the number of hydrogen bonds in the AKT1/TNF complexes was between 1–2 and 2–3 respectively. To gain a more comprehensive understanding of the binding stability of Beta-Sitosterol with AKT1 and TNF, a detailed analysis of the energy contributions was conducted. [Table 9](#) presents the binding free energy analysis results for the Beta-Sitosterol-AKT1/TNF complex, including van der Waals interaction energy ( $\Delta V_{DWAALS}$ ), electrostatic energy ( $\Delta E_{ele}$ ), nonpolar solvation energy ( $\Delta E_{surf}$ ), molecular mechanics energy ( $\Delta G_{gas}$ ), solvation free energy ( $\Delta G_{solvation}$ ), and total binding free energy ( $\Delta G_{bind}$ ). The  $\Delta G_{bind}$  energy, which is the sum of  $\Delta G_{gas}$  and  $\Delta G_{solvation}$ , provides a comprehensive assessment of the binding strength and stability between the molecules. The total binding free energies for the Beta-Sitosterol-AKT1 and Beta-Sitosterol-TNF complexes were  $-26.07$  kcal/mol and  $-40.99$  kcal/mol, respectively. However, a notable disparity is observed between the binding energies obtained from molecular docking (Beta-Sitosterol-AKT1 at  $-11.31$  kcal/mol and Beta-Sitosterol-TNF at  $-9.49$  kcal/mol) and the total binding free energies derived from molecular dynamics simulations. This discrepancy may be attributed to several factors, including differences in initial conformations, solvent effects, temperature and pressure conditions, simulation time, and the choice of force fields and parameters. Specifically, molecular docking is typically carried out in a static environment, whereas molecular dynamics simulations account for the dynamic behavior of molecules in a solvent. In this study, solvent molecules may form additional hydrogen bonds or other

**Table 9** Analysis of Binding Free Energy of the Beta-Sitosterol- AKT1/ TNF Complex (kcal/Mol)

Energy Contributions	AKT1	TNF
$\Delta$ VDWAALS	-43.06	-62.55
$\Delta$ E <sub>ele</sub>	-3.22	-6.41
$\Delta$ E <sub>surf</sub>	-5.47	-7.33
$\Delta$ G <sub>gas</sub>	-46.28	-68.95
$\Delta$ G <sub>solvation</sub>	20.21	27.96
$\Delta$ G <sub>Bind</sub>	-26.07	-40.99

**Abbreviations:**  $\Delta$ VDWAALS, Van der Waals interaction energy;  $\Delta$ E<sub>ele</sub>, Electrostatic energy;  $\Delta$ E<sub>surf</sub>, Nonpolar solvation energy;  $\Delta$ G<sub>gas</sub>, Molecular mechanics energy;  $\Delta$ G<sub>solvation</sub>, Free energy of solvation;  $\Delta$ G<sub>Bind</sub>, Total binding free energy (sum of  $\Delta$ G<sub>gas</sub> and  $\Delta$ G<sub>solvation</sub>).

interactions with Beta-Sitosterol and receptor proteins, consequently affecting the total binding free energy. Furthermore, an elevated temperature may lead to heightened molecular thermal motion, thereby influencing the total binding free energy. Alterations in pressure may also impact the volume and conformation of molecules, thereby influencing the total binding free energy. The results of molecular dynamics simulations indicate that the binding energy of Beta-Sitosterol with TNF is lower, which implies a more stable binding. This phenomenon may be related to the structure of TNF's active site and its interactions with the solvent environment. Although there are disparities between the outcomes of molecular docking and molecular dynamics simulations, both approaches highlight the stability of the Beta-Sitosterol-AKT1/TNF complex. These findings suggest that Beta-Sitosterol holds promise for treating sepsis-induced acute lung injury. Nevertheless, additional experimental data are required to validate its clinical feasibility.

## Results of Cellular Experimental Validation

### Effect of Xijiao Dihuang Decoction on the Viability of Human Type II Alveolar Epithelial A549 Cells

Figure 10 depicts the impact of various concentrations of Xijiao Dihuang decoction (0, 50, 100, 200, 400, 800, and 1000  $\mu$ g/mL) on human type II alveolar epithelial A549 cells. The study revealed that at concentrations of 50, 100, and

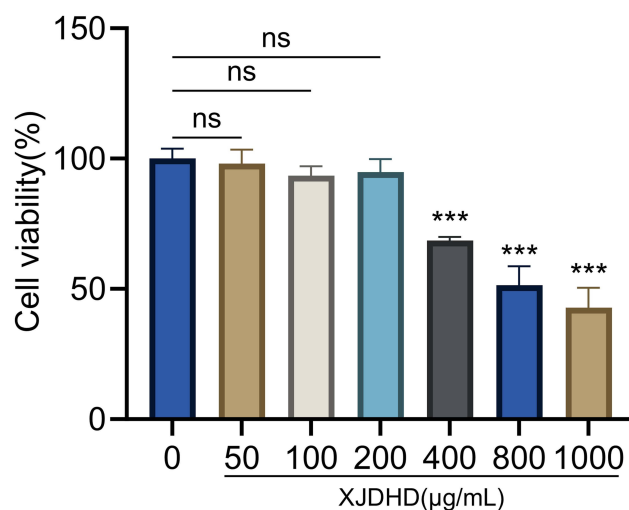


**Figure 10** Presents the impact of XJDHD on the viability of human type II alveolar epithelial A549 cells (mean  $\pm$  standard deviation, n=3). Statistical significance is indicated by asterisks.

**Note:** \*\*\* $p$ <0.001 represent comparisons with the 0  $\mu$ g/mL control group.

**Abbreviations:** ns, no significance.

200 µg/mL, the decoction exhibited minimal influence on cell viability ( $p > 0.05$ ). In contrast, at higher doses of 400, 800, and 1000 µg/mL, a significant decline in cell viability and marked inhibition of cell proliferation were observed ( $p < 0.001$ ). These results indicate that the safe limit for Xijiao Dihuang decoction on A549 cells within 24 hours is 200 µg/mL, as it does not appreciably affect cell viability while maintaining pharmacological activity.

### Effect of Xijiao Dihuang Decoction on LPS-Induced Inflammatory Factor Expression in Human Type II Alveolar Epithelial A549 Cells

As shown in [Figure 11](#) and [Supplementary Table 4](#), the model group exhibited significantly elevated secretion of IL-6, TNF $\alpha$ , and IL-1 $\beta$  in comparison to the control group ( $p < 0.001$ ). To evaluate the effect of Xijiao Dihuang decoction on LPS-induced A549 cells, different concentrations of Xijiao Dihuang decoction were applied. The decoction exhibited a dose-dependent inhibitory effect on the expression of IL-6, TNF $\alpha$ , and IL-1 $\beta$  inflammatory cytokines compared to the model group ( $p < 0.001$ ). Among the treated groups, the XJDH-H group outperformed the XJDH-L group in suppressing the expression of inflammatory factors in LPS-stimulated A549 cells ( $p < 0.001$ ). Collectively, these findings indicate that Xijiao Dihuang decoction effectively counters the inflammatory response in LPS-induced A549 cells by diminishing the expression of such factors.

### Effect of Xijiao Dihuang Decoction on LPS-Induced Oxidative Stress in Human Type II Alveolar Epithelial A549 Cells

As depicted in [Figure 12](#) and [Supplementary Table 5](#), compared to the control group, the model group had a notably elevated MyD88 mRNA expression ( $p < 0.01$ ) and a substantially reduced expression of SOD and CAT mRNAs ( $p < 0.001$ ). Treatment with the high dose XJDH (XJDH-H) led to a significant decline in MyD88 mRNA expression ( $p < 0.05$ ) relative to the model group; however, whereas the low dose XJDH (XJDH-L) did not lead to a statistically significant decrease ( $p > 0.05$ ). Notably, the XJDH-H group's MyD88 mRNA expression showed no significant differences compared with the control group ( $p > 0.05$ ). Both XJDH-L and XJDH-H groups exhibited increased SOD and CAT mRNA levels ( $p < 0.05$ ) compared to the model group, with no significant disparity detected between XJDH-H and the control group ( $p > 0.05$ ). These findings suggest that both dosage levels of XJDH effectively augmented SOD and CAT mRNA expression in LPS-stimulated A549 cells, and the high dose XJDH treatment particularly downregulated MyD88 mRNA, thus mitigating oxidative stress damage in these cells. Additionally, it is worth noting that the lack of a significant reduction in the MyD88 mRNA expression level in the XJDH-L group compared to the model group ( $p > 0.05$ ) may be due to the lower concentration of XJDH-L.

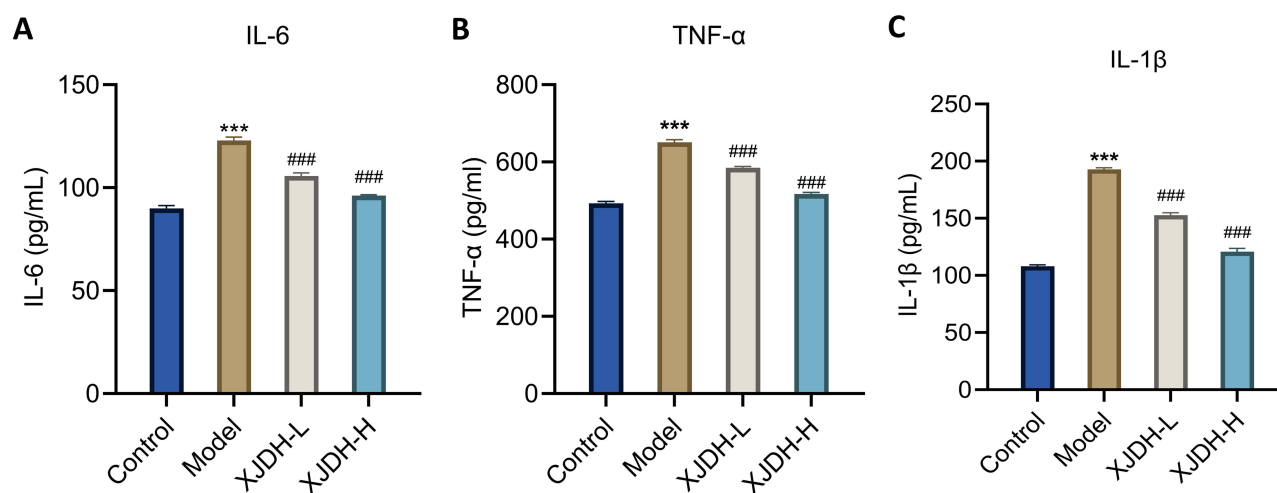


**Figure 11** The impact of XJDHD on the expression of inflammatory cytokines IL-6, TNF $\alpha$ , and IL-1 $\beta$  in LPS-stimulated human type II alveolar epithelial A549 cells. **(A)** Expression levels of IL-6, **(B)** TNF $\alpha$ , and **(C)** IL-1 $\beta$  are presented. The data, presented as mean  $\pm$  standard deviation ( $n=3$ ), demonstrate significant statistical differences. Asterisks denote comparisons with the control group, where

**Notes:** \*\*\* $p < 0.001$  represents highly significant differences. Hash marks denote comparisons with the model group, where ### $p < 0.001$  represents highly significant differences.

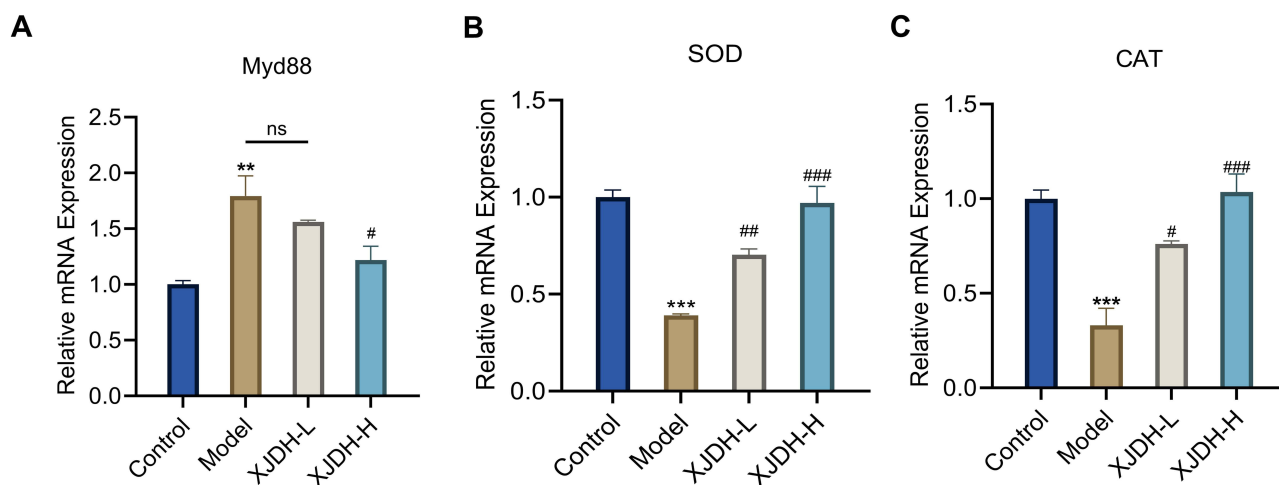


**Figure 12** The impact of XJDHD on the mRNA expression levels of Myd88, SOD, and CAT in LPS-stimulated human type II alveolar epithelial A549 cells (mean ± standard deviation, n=3). (A) Myd88 mRNA expression level, (B) SOD mRNA expression level, (C) CAT mRNA expression levels. Hash marks denote comparisons with the model group, where.

**Note:** #*p*<0.05, ##*p*<0.01, and ###*p*<0.001 represent highly significant differences. Asterisks denote comparisons with the control group, where \*\**p*<0.01 and \*\*\**p*<0.001 represents highly significant differences.

**Abbreviations:** ns, no significance.

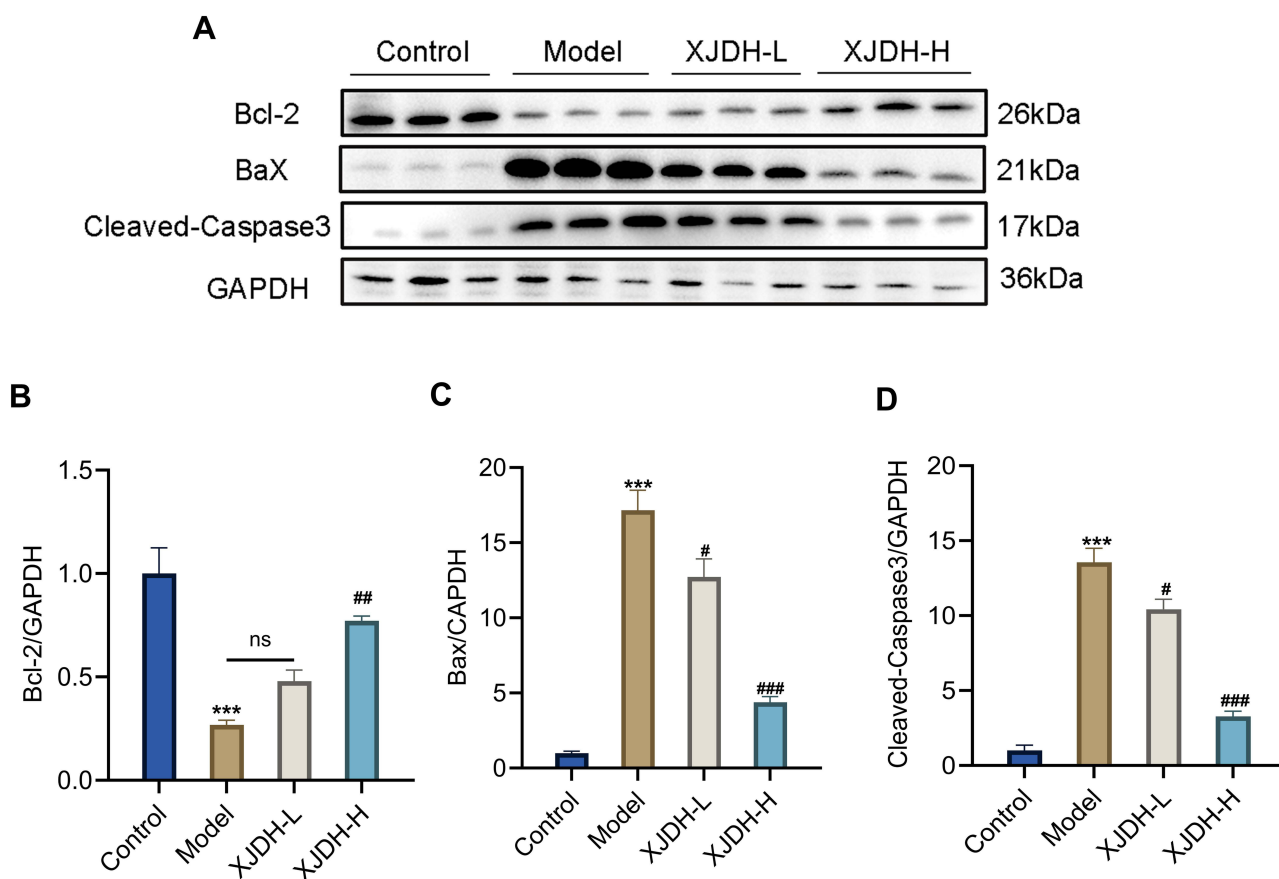


**Figure 13** Investigates the impact of XJDHD on the expression levels of key apoptotic proteins Bax, Bcl-2, and Cleaved-Caspase-3 in human type II alveolar epithelial A549 cells (n=3). GAPDH is used as an internal reference protein. (A) Protein expression levels of Bax, Bcl-2, and Cleaved-Caspase-3 were determined by Western blotting. Quantitative gray-scale densitometry analysis for Bcl-2 (B), Bax (C), and Cleaved-Caspase-3 (D). Hash marks denote comparisons with the model group, where.

**Note:** #*p*<0.05, ##*p*<0.01, and ###*p*<0.001 represent highly significant differences. Asterisks denote comparisons with the control group, where \*\*\**p*<0.001 represents highly significant differences.

**Abbreviations:** ns, no significance.

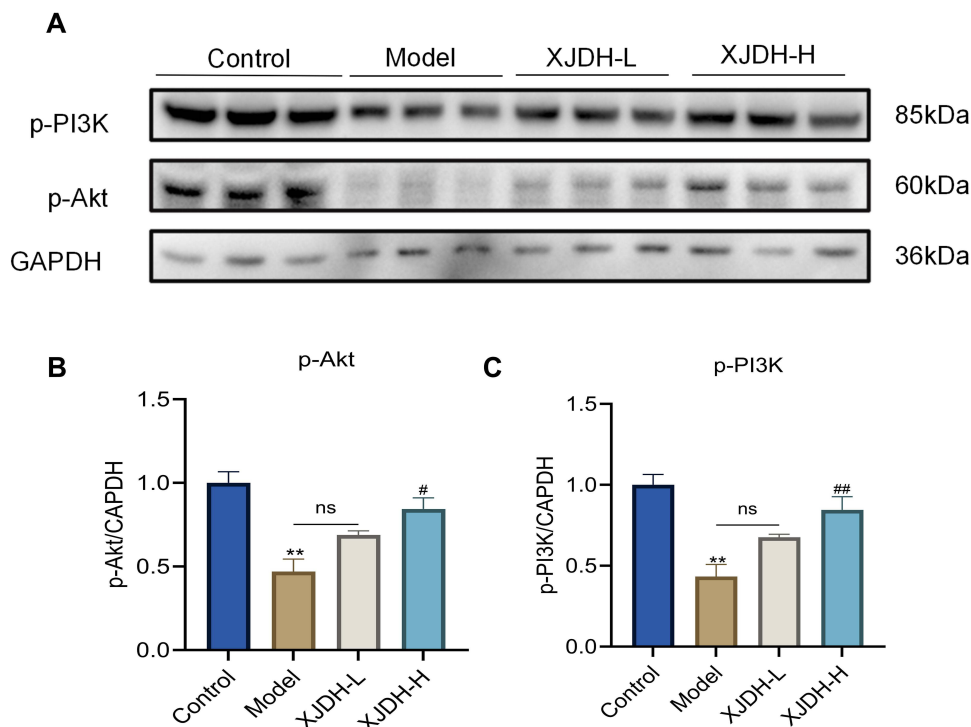


**Figure 14** The impact of XJDHD on the expression levels of p-PI3K and p-Akt apoptotic proteins in human type II alveolar epithelial A549 cells (n=3). GAPDH is used as an internal reference protein for normalization. **(A)** Protein expression levels of p-PI3K and p-Akt were determined by Western blotting. Quantitative gray-scale densitometry analysis for p-Akt **(B)** and p-PI3K **(C)**. Hash marks denote comparisons with the model group, where.

**Notes:** \* $p < 0.05$  and ## $p < 0.01$  represent highly significant differences. Asterisks denote comparisons with the control group, where \*\* $p < 0.01$  represents highly significant differences.

**Abbreviations:** ns, no significance.

### Effects of Xijiao Dihuang Decoction on the Expression Levels of Bax, Bcl-2, and Cleaved-Caspase-3 Apoptotic Proteins in Human Type II Alveolar Epithelial A549 Cells

Figure 13 and Supplementary Table 6 illustrate the examination of apoptosis-related proteins Bax, Bcl-2, and Cleaved-Caspase-3 expression levels to validate network pharmacology and molecular docking findings. Compared to the control group, the model group had significantly increased Bax and Cleaved-Caspase-3 expression ( $p < 0.001$ ) and decreased Bcl-2 expression ( $p < 0.001$ ) in A549 cells. Treatment with XJDH-H and XJDH-L doses led to reduced Cleaved-Caspase-3 and Bax expression ( $p < 0.05$ ) relative to the model group. Notably, Bcl-2 expression significantly rose in the XJDH-H group ( $p < 0.01$ ), whereas in the XJDH-L group, this change did not reach statistical significance ( $p > 0.05$ ). When comparing the XJDH-H and XJDH-L groups, there was a downward trend in Bax and Cleaved-Caspase-3 expression and an upward trend in Bcl-2 expression. Thus, Xijiao Dihuang decoction, predominantly the high-dose group (XJDH-H), demonstrated a superior capacity to alleviate LPS-induced apoptosis in A549 cells. Additionally, the lack of significant difference in the expression level of Bcl-2 between the XJDH-L group and the model group ( $p > 0.05$ ) may be ascribed to the lower concentration of XJDHD. Furthermore, compared to the XJDH-L group, the expression levels of Bax and Cleaved-Caspase-3 in the XJDH-H group showed a decreasing trend, suggesting that the effect of XJDHD on apoptosis-related proteins may be dose-dependent.

### Effect of Xijiao Dihuang Decoction on the Expression Levels of PI3K/Akt Signaling Pathway-Related Proteins in Human Type II Alveolar Epithelial A549 Cells

Figure 14 and Supplementary Table 7 reveal that the expression levels of p-PI3K and p-Akt were notably reduced in A549 cells of the model group compared to the control group ( $p < 0.01$ ). Treatment with high-dose XJDH-H group exhibited significantly increased expression of p-PI3K and p-Akt compared to the model group ( $p < 0.05$ ). In contrast, there was no statistically significant difference in the low-dose XJDH-L group ( $p > 0.05$ ). These findings suggest that Xijiao Dihuang

decoction, especially the high-concentration formulation, has the potential to ameliorate LPS-induced ALI by influencing the PI3K/Akt signaling pathway. Additionally, compared with the model group, the expression levels of p-PI3K and p-Akt in the XJDH-L group did not show significant differences ( $p>0.05$ ), which might be due to the lower concentration of XJDHD.

## Discussion

SALI is a clinical syndrome with a poor prognosis. Its pathogenesis is intricate, and both the morbidity and mortality rates remain elevated, imposing substantial economic and medical burdens. At present, the treatment of SALI in modern medicine mainly encompasses the utilization of broad-spectrum antibiotics, fluid resuscitation, and mechanical ventilation.<sup>34</sup> While these approaches can, to a certain degree, manage infections and sustain vital signs, they might not comprehensively address the inflammation and immune dysregulation that underlie Systemic Acute Lung Injury (SALI). Additionally, these interventions may be accompanied by notable side effects and complications, including secondary infections, heightened antibiotic resistance, and drug-related liver and kidney impairments.<sup>7</sup> Consequently, timely, effective, and safe multi-target and multi-pathway interventions are of utmost importance in alleviating the symptoms of sepsis-induced acute lung injury.

The management of sepsis-induced acute lung injury in the context of traditional Chinese medicine is distinguished by its multifaceted approach, targeting numerous aspects and pathways simultaneously. XJDHD, which is included in Sun Simiao's pharmaceutical classic "Beiji Qianjin Yaofang", is a commonly used formula for the treatment of sepsis. It is composed of four ingredients: Buffalo Horn, Rehmannia, White Paeony Root, and Cortex Moutan. However, the exact mechanism by which Xijiao Dihuang decoction exerted its therapeutic benefits in treating sepsis-induced acute lung injury is still not well understood and requires further exploration.

The treatment of SALI has attracted increasing attention from researchers, leading to numerous studies investigating potential therapeutic agents. In this context, our study aimed to elucidate the underlying mechanism by which the key active components of XJDHD exert their therapeutic effects on SALI. By adopting an integrated approach that encompassed network pharmacology, molecular docking, molecular dynamics simulations, and experimental validation, we sought to conduct a systematic exploration and validation on the efficacy of XJDHD in treating SALI.

Firstly, the TCMSP and HERB databases were used to identify 20 active chemical components and 313 potential gene targets from the four Chinese medicines in XJDHD. Subsequently, 3250 SALI-related gene targets were retrieved from the OMIM and GeneCards databases. By intersecting the disease targets with those of the Chinese medicines, 182 intersecting targets and 17 active chemical components were identified. The main chemical components include Beta-Sitosterol, Cianidanol, Quercetin, and Kaempferol. Beta-Sitosterol, a tetracyclic triterpenoid, has reportedly enhanced recovery from acute lipopolysaccharide-induced lung injury through reducing apoptosis, suppressing inflammation, and mitigating fibrosis.<sup>35</sup> Notably, quercetin, a flavonoid renowned for its potent antioxidant and anti-inflammatory effects, was shown by Sang et al to initiate the SIRT1/AMPK signaling pathway, combating oxidative stress-induced endoplasmic reticulum stress and thus relieving sepsis-induced acute lung injury.<sup>36</sup> Catechins, polyphenolic compounds with antioxidative and anti-inflammatory properties, induce autophagy *in vivo* to decrease lung inflammation in ALI.<sup>37</sup> Kaempferol, a flavonol, efficaciously diminishes polyubiquitination of K63-linked proteins, hence suppressing NF- $\kappa$ B activation and inflammatory responses in mouse models of ALI.<sup>38</sup>

The investigation of the 182 shared targets from GO enrichment and KEGG pathway analyses revealed that XJDHD primarily influences the biological processes of apoptosis and inflammatory response in the treatment of SALI. Key signaling pathways implicated in this process include MAPK, PI3K-Akt, HIF-1, and IL-17 pathways, with the PI3K-Akt pathway emerging as a significant mediator of the acute inflammatory response. Research indicates that the PI3K/Akt signaling cascade is vital for cell growth, apoptosis, metabolism, and immunity.<sup>39</sup> Studies demonstrate that genipin improves lipopolysaccharide (LPS)-induced ALI by mitigating mitochondria-dependent apoptosis and endoplasmic reticulum stress (ERS) via the PI3K/Akt pathway.<sup>40</sup> Artesunate has also displayed potential in preventing LPS-induced ALI by modulating the PI3K/Akt/mTOR axis, reducing apoptosis and inflammatory mediator release.<sup>41</sup> Similarly, ginsenoside GRg1 exerts a protective effect against SALI by inhibiting apoptosis in alveolar epithelial cells and reducing pro-inflammatory cytokine secretion, largely through PI3K-Akt activation.<sup>42</sup> Data suggests that Xijiao Dihuang decoction (XJDHD) significantly amplifies the expression of p-PI3K and p-Akt proteins in LPS-stimulated human type II alveolar

epithelial A549 cells ( $p < 0.05$ ). Specifically, this finding leads to the proposal that XJDHD may alleviate LPS-induced ALI through PI3K/Akt regulation. PPI network analysis unveiled 180 nodes and 3573 edges, highlighting IL6, TNF, AKT1, MMP9, HIF1A, JUN, BCL2, PTGS2, IL1B, and CASP3 as pivotal core hub targets for XJDHD's effectiveness in treating SALI. To confirm the affinity of these core proteins to XJDHD's chemical components, molecular docking and molecular dynamics simulation analyses were conducted. Molecular docking results revealed that the active ingredients, namely beta-sitosterol, cyanidanol, and quercetin, exhibited strong bindings to the core protein targets AKT1, TNF, and PTGS2. The binding energy values were below -9.0 kcal/mol, which implies that a stable chemical structure is formed through their interaction with the target proteins. Therefore, these herbal chemical components may regulate the activity of specific proteins. In this study, through the positive-control group for molecular docking, the binding energies of SC79-AKT1 and SPD304-TNF were determined to be -11.15 kcal/mol and -9.27 kcal/mol, respectively. These results suggest that the binding affinities of Beta-Sitosterol with AKT1 -11.31 kcal/mol and TNF -9.49 kcal/mol are analogous to those of the known positive small-molecule drugs, thus further buttressing the hypothesis that Beta-Sitosterol is a potential active drug targeting AKT1 and TNF. To further verify the stability of the complex and its related biological roles, 100 ns molecular dynamics simulations were conducted on the highest binding energy complexes of Beta-Sitosterol and AKT1/TNF target proteins. The RMSD results showed that, with an RMSD value of less than 1 nm, the overall structure of the Beta-Sitosterol-AKT1/TNF complex remained stable. The RMSF analysis revealed that the Beta-Sitosterol-AKT1/TNF complexes contained large flexible regions. Both complexes exhibited small R(g) values, which is indicative of their compact molecular structures. Moreover, the Beta-Sitosterol-AKT1 and Beta-Sitosterol-TNF complexes had the number of hydrogen bonds ranging from 1 to 2 and 2 to 3, respectively. Based on the Gibbs free energy landscape, both complexes exhibited distinct and concentrated regions of lowest energy, suggesting that they reached an optimal stable state upon binding, with the molecular structures exhibiting a high degree of compactness. The total binding free energy of the Beta-Sitosterol-AKT1/TNF complexes were calculated to be -26.07 kcal/mol and -40.99 kcal/mol, respectively, further indicating that the complexes were more stable. Therefore, the comprehensive molecular dynamics simulation results confirmed that the Beta-Sitosterol-AKT1/TNF complex is structurally stable and has a high potential for biological activity.

To corroborate the findings of network pharmacology, molecular docking, and molecular dynamics, in vitro validation was conducted by stimulating human type II alveolar epithelial A549 cells with LPS to simulate ALI. Firstly, the CCK8 assay demonstrated that a concentration of 200  $\mu\text{g/mL}$  of XJDHD was the maximum safe level at 24 hours, as it had no negative impact on cell viability observed. Secondly, both the XJDH-L and XJDH-H groups were found to reduce the levels of IL-6, TNF $\alpha$ , and IL-1 $\beta$  in LPS-stimulated A549 cells, thereby mitigating the inflammatory response ( $p < 0.001$ ). Furthermore, q-PCR was employed to quantify the levels of SOD, MyD88, and CAT mRNA in LPS-stimulated A549 cells. The results showed that Xijiao Dihuang decoction, particularly the XJDH-H group, effectively decreased MyD88 mRNA expression ( $p < 0.05$ ) and increased SOD and CAT mRNA levels ( $p < 0.05$ ), thereby alleviating oxidative stress. Subsequently, the expression levels of apoptotic proteins in A549 cells were assessed. In the XJDHD groups, particularly in the XJDH-H group, the levels of Bax and Cleaved-Caspase-3 exhibited a downward trend ( $p < 0.05$ ), while the expression of BCL-2 showed an upward trend ( $p < 0.01$ ). This suggests that XJDHD, especially the XJDH-H group, was more effective in mitigating LPS-induced apoptosis in A549 cells.

While these in vitro experiments secure encouraging results, the present study still has several limitations. Firstly, although in vitro experiments have confirmed the anti-inflammatory, antioxidant, and anti-apoptotic effects of XJDHD, these findings have not been verified in animal models or clinical trials. Consequently, future research should focus on developing SALI animal models to evaluate the in vivo efficacy and safety of XJDHD. Secondly, this study primarily focused on the regulatory role of the PI3K/Akt signaling pathway, with a lack on comprehensive exploration of other potential signaling pathways. Future research should further investigate the effects of XJDHD on other signaling pathways to more fully elucidate its therapeutic mechanisms. Additionally, as a traditional Chinese medicine compound, the synergistic mechanisms between the various components of XJDHD remain unclear. Future research is expected to elucidate the specific contributions of each component through monomer preparation. Moreover, the use of in vitro models may be limited by cell type and experimental conditions, potentially affecting the universality and applicability of the results. Therefore, future research endeavors should take into account the utilization of diverse cell types and more

intricate culture conditions to more effectively replicate the clinical milieu. Finally, as a multi-component herbal formulation, XJDHD may pose unresolved safety concerns that remain unelucidated in this investigation. Subsequent studies should incorporate comprehensive safety assessments encompassing toxicological profiling and identification of adverse reactions to ensure clinical safety. In summary, we have undertaken a preliminary investigation of XJDHD's therapeutic potential against SALI utilizing network pharmacology and in vitro experimental approaches. Although these findings lay a groundwork for further research, it is critical to emphasize that XJDHD remains unvalidated in preclinical animal models or human trials. Consequently, these observations must be interpreted as exploratory and warrant rigorous validation through translational studies to establish both scientific rigor and clinical relevance.

## Conclusion

In summary, the mechanisms underlying the alleviation of SALI by XJDHD have been preliminarily explored through the application of network pharmacology, molecular dynamics simulations, and in vitro experiments. The results indicate that XJDHD exerts anti-inflammatory, anti-oxidative stress, and anti-apoptotic effects on alveolar epithelial cells via the PI3K/Akt signaling pathway in a dose-dependent manner. Additionally, a “component-target-pathway” interaction system was constructed, offering preliminary insights into the multi-target effects of XJDHD in the treatment of SALI. However, owing to the disparities among computational simulations, in vitro experimental outcomes, and the in vivo milieu, additional experimental verification is still requisite. To this end, future research not only has to assess the therapeutic effectiveness of XJDHD in animal models and clinical trials, but also ought to utilize multi-omics technologies to explore its potential interactions with other pathways, such as the mitogen-activated protein kinase (MAPK) and hypoxia-inducible factor-1 (HIF-1).

## Data Sharing Statement

The original contributions presented in the study are incorporated within the article or [supplementary material](#). For further inquiries, please direct them to the first author.

## Ethics Declarations

This study does not involve experiments with human or animal subjects; therefore, ethical review is considered unnecessary. In accordance with Articles 1 and 2 of Article 32 of the “Measures for Ethical Review of Life Science and Medical Research Involving Human Subjects,” ethical approval is exempted for this study. Although this study did not involve animal or human subjects and was exempt from ethical review, the ethical guidelines and standards set by our institution and country were strictly followed. The research was conducted in accordance with the principles of the Helsinki Declaration and the guidelines of the Committee on Publication Ethics (COPE). It is hereby confirmed that the research was conducted in compliance with ethical standards and that all data and results are presented accurately and without bias.

## Acknowledgments

The authors would like to express their gratitude to the researchers and staff associated with the aforementioned software and databases.

## Author Contributions

All authors have made substantial contributions to the reported work. These contributions encompass various stages, including conceptualization, design, implementation of the study, data collection, analysis, and interpretation. Each author also participated in drafting, revising, or critically reviewing the manuscript. They have provided their final approval of the version to be published, reached an agreement on the journal for submission, and assume responsibility for all aspects of the work.

## Funding

National Clinical Medical Research Centre for Acupuncture and Moxibustion Open Subjects(NCRCOP2023015).

## Disclosure

The authors declare that no competing interests are involved in this study.

## References

- Liu D, Huang SY, Sun JH, et al. Sepsis-induced immunosuppression: mechanisms, diagnosis and current treatment options. *Military Med Res.* 2022;9(1):56. doi:10.1186/s40779-022-00422-y
- Qing Z, Yixue Z, Yang L, et al. Progress in the study of pathophysiological mechanisms of sepsis. *Chin J Hosp Infect.* 2022;32(16):2551–2555. doi:10.11816/cn.ni.2022-220242
- Jianfeng X, Hongliang W, Kang Y, et al. the epidemiology of sepsis in Chinese ICUs: a national cross-sectional survey. *Crit Care Med.* 2020;48(3):e209–e218. doi:10.1097/CCM.0000000000004155
- Fan EKY, Fan J. Regulation of alveolar macrophage death in acute lung inflammation. *Respir Res.* 2018;19(1):50. doi:10.1186/s12931-018-0756-5
- Shen Y, He Y, Pan Y, et al. Role and mechanisms of autophagy, ferroptosis, and pyroptosis in sepsis-induced acute lung injury. *Front Pharmacol.* 2024;15:1415145. doi:10.3389/fphar.2024.1415145
- He W, Xi Q, Cui H, et al. Liang-Ge decoction ameliorates acute lung injury in septic model rats through reducing inflammatory response, oxidative stress, apoptosis, and modulating host metabolism. apoptosis, and modulating host metabolism. *Front Pharmacol.* 2022;13:926134. doi:10.3389/fphar.2022.926134
- Cecconi M, Evans L, Levy M, et al. Sepsis and septic shock. *Lancet.* 2018;392(10141):75–87. doi:10.1016/S0140-6736(18)30696-2
- Wen C, Fenghua Q, Qi S, et al. Clinical study on the intervention of sepsis-induced acute lung injury prognosis by sini shengjiang powder through modulating the liver-spleen axis. *J Emerg Traditi Chin Med.* 2024;33(11):1929–1933. doi:10.3969/j.issn.1004-745X.2024.11.010
- Dexiang W, Jiawen Y, Qinyun L, et al. Influences of treatment timing of the TCM prescription qingfei huayu tongfu formula on the therapeutic effect and prognosis of sepsis-related acute respiratory distress syndrome. *China General Practice.* 2025;1–6. doi:10.12114/j.issn.1007-9572.2024.0107
- Chenfei F, Qun L, Guangjun W, et al. Research progress of Chinese medicine in preventing acute lung injury in sepsis. *China TCM Emergencies.* 2024;33(01):169–171+185. doi:10.3969/j.issn.1004-745X.2024.01.045
- Song Y, Lin W, Zhu W. Traditional Chinese medicine for treatment of sepsis and related multi-organ injury. *Front Pharmacol.* 2023;14:1003658. doi:10.3389/fphar.2023.1003658
- Wang XH, Xu DQ, Chen YY, et al. Traditional Chinese Medicine: a promising strategy to regulate inflammation, intestinal disorders and impaired immune function due to sepsis. *Front Pharmacol.* 2022;13:952938. doi:10.3389/fphar.2022.952938
- Hongyu W, Yanzhong Y, Min L, et al. Progress of research on the treatment of infectious diseases with rhinoceros horn di Huang Tang. *J Liaoning Coll Trad Chin Med.* 2024;1–12.
- Hongyu W, Yanzhong Y, Min L, et al. The impact of xijiao dihuang decoction on coagulation and hemorheology in patients with sepsis-induced coagulopathy and blood-heat syndrome. *Hunan Univ Chin Med.* 2022. doi:10.27138/d.cnki.ghuzc.2022.000284
- Tailiang H. Effect of vitamin C combined with Xijiao Dihuang Decoction on prevention and treatment of sepsis complicated with DIC. *J of China Prescription Drug.* 2023;21(2):110–113. doi:10.3969/j.issn.1671-945X.2023.02.033
- Yuan Z, Deng L, Rong S. Study on the mechanism of xijiao dihuang decoction inhibiting pyroptosis—related proteins in alleviating acute lung injury induced by sepsis. *J Emerg Traditi Chin Med.* 2024;33(3):405–408,414. doi:10.3969/j.issn.1004-745X.2024.03.006
- Liu J, Li Z, Lao Y, et al. Network pharmacology, molecular docking, and experimental verification reveal the mechanism of San-Huang decoction in treating acute kidney injury. *Front Pharmacol.* 2023;14:1060464. doi:10.3389/fphar.2023.1060464
- Yu Z, Ruiting H, Qingwei Z. Exploring the mechanism of action of phlegm-heat-clearing injection in the treatment of acute lung injury based on network pharmacology and molecular docking technology. *Chin J Trad Chin Med.* 2021;46(15):3960–3969. doi:10.19540/j.cnkicjcm.20210406.402
- Sun A, Li YF, Miao Y, et al. Research on the mechanism of Ursolic acid for treating Parkinson's disease by network pharmacology and experimental verification. *Heliyon.* 2024;10(14):e34113. doi:10.1016/j.heliyon.2024.e34113
- Ru J, Li P, Wang J, et al. TCMSP: a database of systems pharmacology for drug discovery from herbal medicines. *J Cheminf.* 2014;6:13. doi:10.1186/1758-2946-6-13
- Fang S, Dong L, Liu L, et al. HERB: a high-throughput experiment- and reference-guided database of traditional Chinese medicine. *Nucleic Acids Res.* 2021;49(D1):D1197–D1206. doi:10.1093/nar/gkaa1063
- Hui L, Jinan W, Wei Z, et al. Systems approaches and polypharmacology for drug discovery from herbal medicines: an example using licorice. *J Ethnopharmacol.* 2013;146(3):773–793. doi:10.1016/j.jep.2013.02.004
- Daina A, Michielin O, Zoete V. SwissTargetPrediction: updated data and new features for efficient prediction of protein targets of small molecules. *Nucleic Acids Res.* 2019;47(W1):W357–W364. doi:10.1093/nar/gkz382
- Kim S, Chen J, Cheng T, et al. PubChem 2023 update. *Nucleic Acids Res.* 2023;51(D1):D1373–D1380. doi:10.1093/nar/gkac956
- Consortium U, Martin M-J, Orchard S. UniProt: the universal protein knowledgebase in 2023. *Nucleic Acids Res.* 2023;51(D1):D523–D531. doi:10.1093/nar/gkac1052
- Stelzer G, Rosen R, Plaschkes I, et al. The genecards suite: from gene data mining to disease genome sequence analyses. *Curr protoc bioinf.* 2016;54:1.30.1–1.30.33. doi:10.1002/cpbi.5
- Philippe B, Jérôme M, Frédéric E, et al. jvenn: an interactive Venn diagram viewer. *BMC Bioinf.* 2014;15:293. doi:10.1186/1471-2105-15-293
- Szklarczyk D, L GA, C NK, et al. The STRING database in 2021: customizable protein-protein networks, and functional characterization of user-uploaded gene/measurement sets. *Nucleic Acids Res.* 2021;49:D605–D612. doi:10.1093/nar/gkaa1074
- Huang DW, Sherman BT, Lempicki RA. Systematic and integrative analysis of large gene lists using DAVID bioinformatics resources. *Nature Protocols.* 2009;4:44–57. doi:10.1038/nprot.2008.211
- Der Spoel D V, Lindahl E, Hess B, et al. GROMACS: fast, flexible, and free. *J Comput Chem.* 2005;26(16):1701–1718. doi:10.1038/nprot.2008.211

31. J AM, Murtola T, Schulz R, et al. GROMACS: high performance molecular simulations through multi-level parallelism from laptops to supercomputers. *SoftwareX*. 2015;1:19–25. doi:10.1016/j.softx.2015.06.001
32. Gopallawa I, E KL, D AN, et al. Small-molecule Akt-activation in airway cells induces NO production and reduces IL-8 transcription through Nrf-2. *Respir Res*. 2021;22(1):267. doi:10.1186/s12931-021-01865-y
33. Mascret A, Mouhsine H, Attia G, et al. New contributions to the drug profile of TNF $\alpha$  inhibitor SPD304: affinity, selectivity and ADMET considerations. *Eur J Pharmacol*. 2021;907:174285. doi:10.1016/j.ejphar.2021.174285
34. Ximo W, Jianbo Y, Shengwei J, et al. expert consensus on the diagnosis and treatment of sepsis-induced pulmonary injury by integrated traditional Chinese and Western Medicine. *Chinese. J Integr Surg Med*. 2020;26(03):400–408. doi:10.3969/j.issn.1007-6948.2020.03.002
35. Qiang Z, Kun Z, Fuqiang L, et al.  $\beta$ -Sitosterol alleviates LPS-induced inflammatory response and fibrosis in rats with acute lung injury *Western Med*. 2022;34(06):813–818. DOI:10.3969/j.issn.1672-3511.2022.06.007
36. Sang A, Wang Y, Wang S, et al. Quercetin attenuates sepsis-induced acute lung injury via suppressing oxidative stress-mediated ER stress through activation of SIRT1/AMPK pathways. *Cell Signalling*. 2022;96:110363. doi:10.1016/j.cellsig.2022.110363
37. C YC, J WC, Y CC, et al. Green tea polyphenol catechins inhibit coronavirus replication and potentiate the adaptive immunity and autophagy-dependent protective mechanism to improve acute lung injury in mice. *Antioxidants*. 2021;10(6):928. doi:10.3390/antiox10060928
38. Qian J, Chen X, Chen X, et al. Kaempferol reduces K63-linked polyubiquitination to inhibit nuclear factor- $\kappa$ B and inflammatory responses in acute lung injury in mice. *Toxicol Lett*. 2019;306:53–60. doi:10.1016/j.toxlet.2019.02.005
39. He X, Li Y, Deng B, et al. The PI3K/AKT signalling pathway in inflammation, cell death and glial scar formation after traumatic spinal cord injury. *Mechanisms Ther Opportunities Cell Prolif*. 2022;55(9):e13275. doi:10.1111/cpr.13275
40. Luo X, Lin B, Gao Y, et al. Genipin attenuates mitochondrial-dependent apoptosis, endoplasmic reticulum stress, and inflammation via the PI3K/AKT pathway in acute lung injury. *Int Immunopharmacol*. 2019;76:105842. doi:10.1016/j.intimp.2019.105842
41. Zhang E, Wang J, Chen Q, et al. Artesunate ameliorates sepsis-induced acute lung injury by activating the mTOR/AKT/PI3K axis. *Gene*. 2020;759:144969. doi:10.1016/j.gene.2020.144969
42. Zhong K, Huang Y, Chen R, et al. The protective effect of ginsenoside Rg1 against sepsis-induced lung injury through PI3K-Akt pathway: insights from molecular dynamics simulation and experimental validation. *Sci Rep*. 2024;14(1):16071. doi:10.1038/s41598-024-66908-y

Journal of Inflammation Research

Publish your work in this journal

The Journal of Inflammation Research is an international, peer-reviewed open-access journal that welcomes laboratory and clinical findings on the molecular basis, cell biology and pharmacology of inflammation including original research, reviews, symposium reports, hypothesis formation and commentaries on: acute/chronic inflammation; mediators of inflammation; cellular processes; molecular mechanisms; pharmacology and novel anti-inflammatory drugs; clinical conditions involving inflammation. The manuscript management system is completely online and includes a very quick and fair peer-review system. Visit <http://www.dovepress.com/testimonials.php> to read real quotes from published authors.

Submit your manuscript here: <https://www.dovepress.com/journal-of-inflammation-research-journal>

**Dovepress**  
Taylor & Francis Group